Wake-Up Transceiver Architectures with Novel Symbol Time Synchronization Schemes for ElectroMagnetic NanoNetworks

Final Year Project

Escola Tècnica Superior de Telecomunicacions de Barcelona (ETSETB)

Author:
Raül Gómez Cid-Fuentes

Advisor:
Dr. Ian F. Akyildiz

July 4, 2011

"If you have heard this story before,
don't stop me, because I'd like to hear it
again"
– Groucho Marx

Acknowledgements

I would like to dedicate a few lines to everyone who has made possible this thesis, to everyone who has supported me and contributed to make the stay in Georgia Institute of Technology my "American dream". First of all, I would like to express my deep gratitude to Professor Ian F. Akyildiz for giving me the chance of coming to his lab, for his very valuable and always helpful advices and also for taking me in his big family. Without him, this thesis would not have been possible.

Secondly, I would like to sincerely thank Professor Eduard Alarcón and Josep Solé, as well as other faculties of UPC for making possible the chance of visiting Georgia Institute of Technology, the Broadband Wireless Laboratory and the reknown Professor Ian F. Akyildiz. Thanks to them for getting, through them, the economical support of Obra Social Bancaja, AGAUR, and ETSETB.

I would also like to thank all the members in the nano-group (Josep M. Jornet, Massimiliano Pierobon, Joan Capdevila, Francesco Rocca Cirasa, Albert Mestres and Sam Meng). Without you all, the way would have been longer and tougher and less exciting. Thank you for your feedback and support. I do not want to forget about the rest of the lab members, outstanding people, professional and charming. I have never met people like all of you. Thank you for making me feel part of a big family.

In these lines, I cannot forget my "family abroad" (Autumn, Umberto and Marie), you have made the best of my stay, we have laughed, shared and been happy altogether. I would have never expected to find anyone like you. Thank you. I have also to thank every one abroad who helped me in the toughest moments and have cheered me up every time I needed. Thank you, Atlanta.

I would also like to appreciate everyone I met during my 5 years in UPC. Several classmates and friends. We have been sharing moments and helping each other every time we needed.

Last but not least, I would like to dedicate some words to my family. Thank you for the infinite support you have given to me and all the love I have gotten from you. Thank you a lot, everything I am, I owe to you.

Abstract

Nanotechnology is enabling new architectures for small-size, low-power, high speed and self-configurable systems. These systems are leading into the design of devices just a few nanometers in size. Among others, applications for nanonsensors in the biomedical, environmental or military fields have been widely explored.

The tasks that theses nanodevices, which are expected to be strongly limited not only in capabilities but also in energy, are limited in performance and complexity. Communications among nodes will expand the applications and capabilities of a single nanodevice through the collaborative effort. This paradigm can provide high complexity in a distributed manner to cover large areas.

The communications alternatives for nano-devices are very limited. Focusing in electromagnetic (EM) paradigm, novel nanomaterials such as graphene are enabling the development of miniaturized EM systems, which set the Terahertz band (0.1 - 10.0 THz) as the expected frequency range of operation for the future EM nanocommunications.

The Time-Spread On Off Keying (TS-OOK) is a modulation that using femtosecond-long pulses concentrates the main frequency components in the Terahertz band and provides almost orthogonal channels to each user.

In this context The work we present on this thesis covers unresolved PHY-Layer topics that covers the transceiver architecture, frequency estimation for symbol synchronization and a wake-up receiver module for node synchronziation. Solving these PHY-Layer topics leads to stablish a base to propose and design network protocols on top of a well-defined architecture.

The main novelty of this transceiver architecture lies on the symbol detection. The proposed transceiver is based on a continuous-time symbol detection, that simplifies the transceiver block diagram, relaxes the synchronization conditions and outperforms existing transceiver architectures proposed in other communication schemes over the Terahertz channel in terms of Symbol Error Rate (SER).

The evaluation of this transceiver architecture is done under the hypothesis that perfect synchronzation is achieved. However, since no nanocrystals are currently reported in the literature, a frequency estimation scheme on built on top of this receiver is proposed. This synchronization scheme takes advantage of the specific properties of the transceiver proposed and it is divided into two stages: a first stage where the receiver estimates the symbol rate using a very short pulse preamble and a second stage where the receiver adaptively corrects the estimation errors and estimates the arrival of the following symbol. The performance of the transceiver is presented in terms of packet error rate (PER) and compared to an analogous transceiver with ideal synchronization.

The energy constraints of the nanodevices create the necessity to activate the transceiver only when a new packet must be sent or received. The lack of nanocrystal oscillators and the fact that OFF-state is a valid state for nanodevices difficult the synchronization between devices. Determining when the nodes must switch on and off cannot be done using current techniques based on duty cycle. The Wake-Up module included in the receiver provides an asynchronous framework to activate selected nodes when a new packet is ready to be sent. This wake-up module defines an asynchronous synchronization protocol for EM nanonetworks. Its performance is evaluated in terms of Energy per bit, delay and throughput.

Contents

List of Figures

Chapter 1

Introduction to Nanonetworks

Wireless Sensor Network (WSN) have been considered as the communication paradigm of the last decade. Several advances in Micro-Electro-Mechanical System (MEMS) technology, wireless communications and digital electronics enabled the production of small devices with sensing capabilities that using the collaborative effort between tens or hundreds of them the performance of the system could be boosted giving way to smart environments [6].

The reduced sensing resolution, the size, still too big to consider them as non-invasive sensors, the energy limitations and energy efficiency of the communication schemes present a bottleneck in this communication paradigm and leads to consider new technologies in the sensing and communication paradigms.

In this context we expect nanotechnology to be the key enabling technology for the development of novel devices and networks. This technology will provide small-size, low-power, high-speed switching and non-invasive devices in a few hundreds of nanometers in size. The tasks that an individual nanodevice can accomplish are limited in terms of complexity. However, the communication among these nanodevices will expand the capabilities of a single nanodevice through collaborative effort. This paradigm can provide high complexity applications in a distributed manner over larger areas [1].

1.1 Nanotechnology, Nanodevices and Applications

In 1959, the Nobel laureate physicist Richard Feynman, in his famous speech "There's Plenty of Room at the Bottom" described for first time, in a top-down approach, how the manipulation of individual atoms or molecules would provide more functional man-made devices. However, it was not until 1974 when Norio Taniguchi first defined nanotechnology as: *Nanotechnology mainly consists of the processing of separation, consolidation and deformation of materials by one atom or one molecule* [7]. This was the first time the term *Nanotechnology* was used. However, in 1996, the Nobel Laureate (Chemistry) Dr. Robert Floyd Curl

Jr. determined that two thousand years ago, Indians were already using nanotechnology processes [8] in the steel manufacture.

Ancient Indian were using nanotechnology to manufacture Wootz steel, also referred as Damascus steel. This steel was characterized by a pattern of bands of sheets of micro carbids and the applications, such as blades, presented a huge toughness [9].

1.1.1 Nanotechnology

More than half a century later from the first speech, the term nanotechnology is also generally used to refer new materials or devices with structures sized from to one to hundreds of nanometers. This nanotechnology is providing a new set of tools to the engineering community to design and manufacture devices in the nanoscale which, for the time being, are only able to perform very simple tasks. Nanotechnology is also enabling miniaturization in the current electronic devices and offers the possibility of interacting with the biological and non-biological nanoscale. Thus, nanotechnology opens a broad field of applications that were not available with previous technologies.

One of the applications is in the field of nanosensing [10, 11, 12, 13]. A nanosensor is a device that can detect new types of events available in the nanoscale. These nanosensors are able to detect the presence of virus, bacteria or cancerous cells [14, 15] in very low concentrations, up to one part per billion [16, 17], . However, the sensing range of these nanosensors is very limited and covers only its close environment. To boost the performance of the nanosensors and to cover large areas, several nanosensors must be deployed over the area to monitor.

To coordinate these nanosensors, we need interaction among them. Amongst others, wireless nanosensor networks provides a framework to enable the communication of nanosensors. To enable this communication paradigm, each one of these nanosensors need, at least, a nanosensing unit to gather the information, a processing unit to interpret the sensed magnitude and a mechanism to report the sensed data to a central unit. These nodes are usually referred as nanodevices.

1.1.2 Nanodevices

We define a nanodevice as an integrated device of around 10-100 μm^2 in size with very simple and limited capabilities. Nanodevices are able to process the information received from the nanosensors and forward this information from one node to another. Nanotechnology provides a vast set of tools for the design of these nanodevices, and although no nanodevices are yet defined, different disciplines (chemical, physical, electrical, biological) converge to the same conclusion in size and capabilities.

In this work, we focus on the Electromagnetic (EM) alternative. We envision that the recent studies on nanomaterials, such as graphene or carbon nanotubes [18], play a key role

in the future development of these nanodevices and provide a more than likely base for the nanonetworking paradigm.

Following the EM approach, the authors in [1] proposed the following architecture for a nanodevice. This architecture is shown in Fig. 1.1 and provides the first attempt to describe in several autonomous blocks the expected operation of a nanodevice. In the following paragraphs we proceed to describe this architecture model.

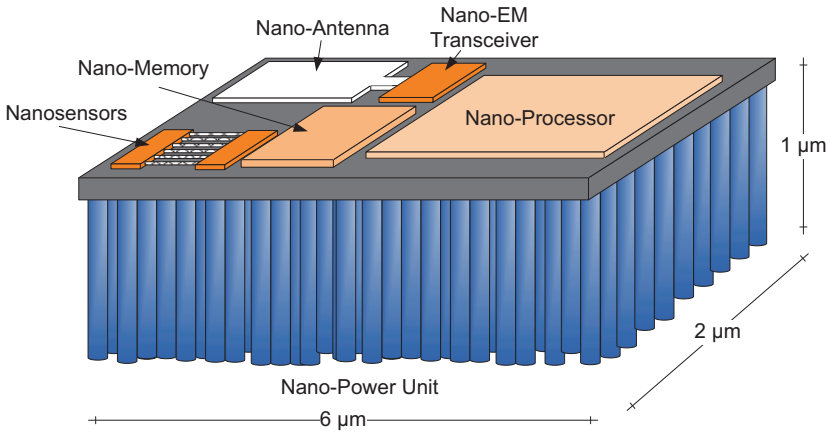

Figure 1.1: Components of a nanosensor device [1].

Nanosensors Unit

Recent developments in nanomaterials, such as graphene are enabling the realization of Carbon Nanotube (CNT) and Graphene Nanoribbon (GNR) technologies [19]. These novel nanomaterials provide excellent sensing capabilities and set the basis for many types of sensors [20] that according to their nature, they can be classified as physical, chemical or biological.

As an example, Fig. 1.2 shows the working principle of CNT Field-Effect Transistor (CNT-FET) based nanosensor under physical, chemical and biological perturbations. In any case, when the CNT is directly affected by the perturbation, it modifies the electrical properties of the transistor.

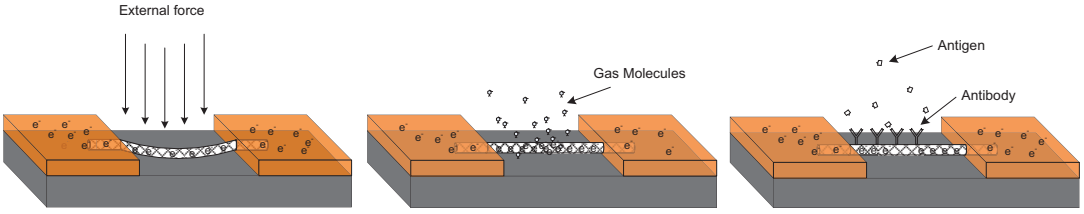

(a) Physical perturbation (b) Chemical perturbation (c) Biological perturbation

Figure 1.2: Illustration of the CNT-FET based nanosensors [1].

Nanoactuator Unit

This unit permits the interaction between the nanodevice and its close environment. Similar to nanosensors, nanoactuators can be classified in physical, chemical and biological [21]. As an example of a physical actuator, Fig. 1.3 shows the working principle of a NEMS where the electrical power is transduced into mechanical movement or deformation of the nanotube. As an example of chemical actuators, we find in [22] a nanoactuator for drug delivering systems.

The nanoactuator field is still in a very early stage of development compared to nanosensors or other units of the nanodevices. However, this unit is not mandatory in the general architecture of a nanodevice. In sensor networks for monitoring purpose only, the nanoactuator unit is not included.

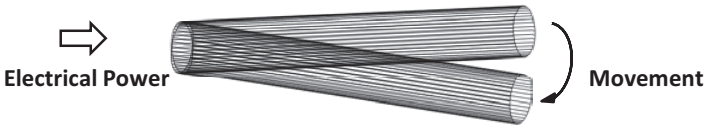

Figure 1.3: Working principle of a NEMS actuator.

Nano-Processor Unit

Recent advances in the miniaturization of Field-Effect Transistor (FET) are leading to new technologies in nanomaterials and new fabrication process that are enabling the future development of processors in the nanoscale. The use of new nanomaterials, such as CNT or GNR, is providing transistors in the nanoscale that are able to operate at ultra high frequencies. Up to now, the fastest FET has been produced by IBM, using graphene technology achieving operation frequencies of up to 155 gigahertz [23]. Alternatively, Single Electron Transistor (SET) is enabling incredible size reduction. In particular, authors in [24] have recently developed a 1.5 nm SET.

Nano-Memory Unit

Memories that stores only one electron per bit suppose the main challenge in nanomemories. The concept of atomic memories was first introduced by R. Feynman in his visionary talk entitled *"There's Plenty of Room at the Bottom"* in 1959. Authors in [24, 25] pave the way for future single electron memories. However there is a long way to go before having atomic memories suitable for chip integration.

Nano-Antenna Unit

The size reduction of classical antennas to sizes of few hundreds of nanometers would require the use of extremely high operating frequencies. The novel properties of graphene-based nano-

antennas reduces significantly the operating frequency and fixes the Terahertz Band as the operating frequency. Nano-antennas have been already proposed in [2, 26].

Nano-EM Transceiver Unit

The EM transceiver of a nanodevice will provide the necessary circuitry to provide the signal processing, frequency conversion, modulation, filtering, amplification, symbol detection and decoding. Since the nano-antenna has been already studied and its operating frequency is set to the Terahertz Band, the RF transistors and circuitry proposed in this unit must be able to operate at Terahertz frequencies.

Nano-Power Unit

In WSN, power management has become the bottleneck in the deployment of extensive networks. In the nanoscale, the power management is expected to be one of the main challenges in the nanonetworks paradigm. However, the expected size reduction of each and every one of the blocks implicitly implies a power reduction in several orders of magnitude. Nanomaterials can be used to manufacture nanobatteries with high power density [27]. Alternatively, novel ultra-nano-capacitors based on Onion-Like-Carbon (OLC) have been recently explored [28]. These capacitors support very fast charging and discharging rates, well supporting pulsed energy fluctuations. They have a very large specific capacity and they resist millions of charging and discharging cycles.

The total amount of energy that a nanobattery or a nanocapacitor of a few hundreds of nanometers in size can store is very limited. Thus, EM nanonetworks must base their working principle in nanoscale energy harvesting. Zinc Oxide (ZnO) nanowires present promising properties in the future development of nanoscale energy harvesters [29, 30].

1.1.3 Applications

Wireless NanoSensor Networks (WNSNs) have a vast amount of applications in which sensor networks cannot apply. These new applications ranges from intra-body applications to non-invasive applications. We classify these applications into the following four groups:

Biomedical Applications

Intra-body cells and organelles are naturally located in the nanoscale. Nanodevices of few hundreds of nanometers in size can provide bio-compatibility and provide a very large number of applications in this field. Several biological nanosensors for medical applications are being investigated. These sensors can either be deployed over or inside the body to detect glucose, sodium or cholesterol [31, 32] and also to detect infections or cancer tissue [33]. A wireless

interface such as a cell phone can be use to collect the information from the sensors and report it to the health care center.

Environmental Applications

Applications for trees, herbs, bushes or plants. amongst others, releasing composites and control for plantations [34, 35]. Nanosensors for other applications in pollution control or biodegradation are also of research interest [11].

Industrial and Consumer Goods Applications

Creation of smart environments, automatic control of the temperature, self-cleaning nanomaterials fibers and textiles, are some of the many examples of the WNSNs. These nanonetworks with direct applications in the consumer goods applications points directly to the recently introduced term Internet of Nano-Things [36].

Military Applications

Advanced Nuclear, Biological and Chemical (NBC) defenses, and sophisticated control and damage systems are examples of military applications. Drug releasing for military applications is also a good example where the soldier receives instantaneous drug to improve his performance in the battlefield.

1.2 Electromagnetic Nanonetworks

In the previous section we have defined the nanodevices as not only tiny devices, but also nanoscale units able to perform simple tasks and communicate among them. Jointly with the simple tasks that these nanodevices can perform, their interaction with the environment is constrained to a very short distance.

In order to broad the applications and boost the performance of these nanodevices, the use of nanonetworks has been discussed in [1]. Setting up a communication paradigm among these devices, nanodevices can perform more complex tasks in a distributed manner and extend the range of influence from the close environment of a device to cover large areas. We expect that the communication among devices will expand the possibilities and applications of nanotechnology.

The strong limitations and constraints of nanodevices reduces the communication range between nodes in up to tens of millimeters. For this, classical existing communication paradigms cannot be directly applied to this field. Amongst others, the main communication paradigms in the nanoscale are the bio-inspired Molecular Communications [37] and the EM communications [1].

- *Molecular Communications:* this is defined as the transmission and reception of encoded information into molecules [37, 38, 39]. This biological approach can be divided by several factors, but we consider that a distance range is a good factor to classify them. Fig. 1.4 shows this classification in short, medium and long range. In [40], a channel model for this diffusion-based molecular communication is provided.

- *Electromagnetic Communications:* This is defined as the exchange of information through electromagnetic radiation, based on novel nanomaterials and their properties. This communication paradigm is set as starting point. As follows, a detailed description, covering technology exploration, radiation in the Terahertz using nanodevices and its propagation model and the basic modulations provided to guarantee an point-to-point communication.

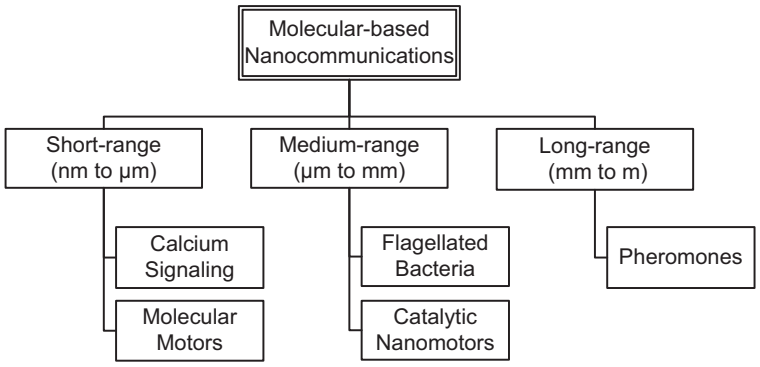

Figure 1.4: Classification of different molecular communication techniques according to the distance.

1.2.1 Technology Exploration for EM Nanonetworks

There is still a long way to go before nanodevices can be developed. Nanotechnology is starting to provide promising results. In the following paragraphs we provide an exploration of novel electromagnetic technologies that we expect that will influence the development of future nanodevices and nanonetworks.

Graphene

Graphene is a one-atom-thick planar sheet of carbon atoms which are densely packed in a honeycomb crystal lattice, see Fig. 1.5. It is because of this honeycomb 2D structure that electrons moves in the material like if they have no mass. This cause electrons to move in Graphene at velocities 300 times less than the light speed in the vacuum [41]. This peculiar property hints at the idea that the transmission and radiation properties will be influenced by this changes of velocities. Moreover, the ballistic conductance of Graphene, electrons

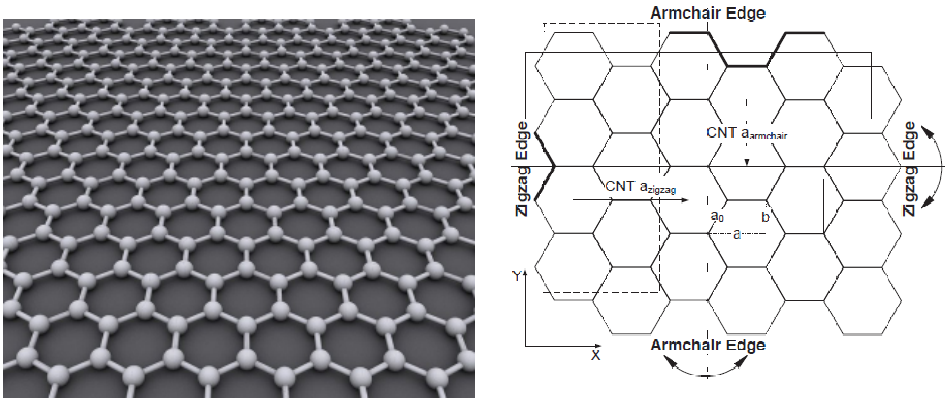

Figure 1.5: Graphene: one-atom-thick planar sheet of carbon atoms [2] .

traveling large distances without being scattered, points also at the fact that Graphene-based electronics will be less noisy and hence much more faster.

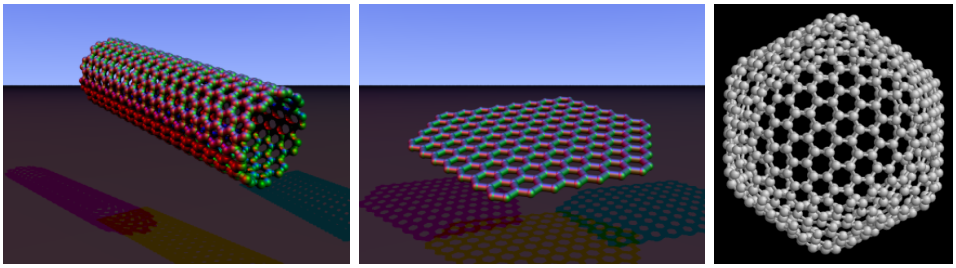

Figure 1.6: Graphene allotropes (CNT, GNR, Sphere Fullerenes) .

Different forms of Graphene, also called allotropes, can be found in the nature or even can be artificially grown by means of chemical processes. The properties of these new nanomaterials is determined by the way Graphene is cut and wrapped. Some of the most known Graphene allotropes are shown in Fig. 1.6 and their features are described in what follows.

- CNTs are cylindrical allotropes of Graphene which are built from rolling Graphene sheets in a given direction. Depending on the bending direction; we differentiate between zigzag, armchair or chiral nanotubes, see Fig. 1.6 on the left. The electronic properties of these components are also related with the bending direction in the rolling process. Furthermore, there also exist single-walled and multi-walled nanotubes. While Single-walled Nanotubes (SWNTs) are constituted by only one rolled sheet of Graphene with a diameter closed to 1 nm, Multi-walled Nanotubes (MWNTs) are composed of several concentric rolled sheets of Graphene.

- GNRs are strips of Graphene with armchair or zigzag edges, see Fig. 1.6 in the middle. The type of edges plays a key role in the electronic properties of these components. While zigzag GNRs are always metallic, armchair GNRs can be either metallic or semiconducting depending on their width. Grosse *et. al*, researchers from the University of Illinois, have recently discovered that this novel nanomaterial is able to reabsorb a

great part of the heat produced by itself [42]. This phenomenon is commonly referred as the *Self-Cooling* effect in graphene and provides an unexpected increase in the energy efficiency of the nanomaterial. Alternatively, this effect removes the necessity of using cooler or dissipation circuits. This reduces the size and enables the development of 3D structures which can improve the future capabilities in the nanoscale.

- Sphere Fullerenes or Buckyballs are spherical allotropes of Graphene composed by several carbon atoms tight each other, see Fig. 1.6 on the right. For instance, C_{60} is a truncated icosahedron with 60 carbon atoms and 20 bonds. The peculiar properties of these allotropes make them attractive for medical applications to target resistant bacteria or even certain types of cancers [43].

Electronic Applications of Graphene Technology

Influenced by the ambipolarity of graphene, graphene transistors provide a different response to a same input excitation than previous electronic circuits. These different behavior leads to redefine the basic cells in the electronic design. We divide the impact of graphene in the electronics into two main groups:

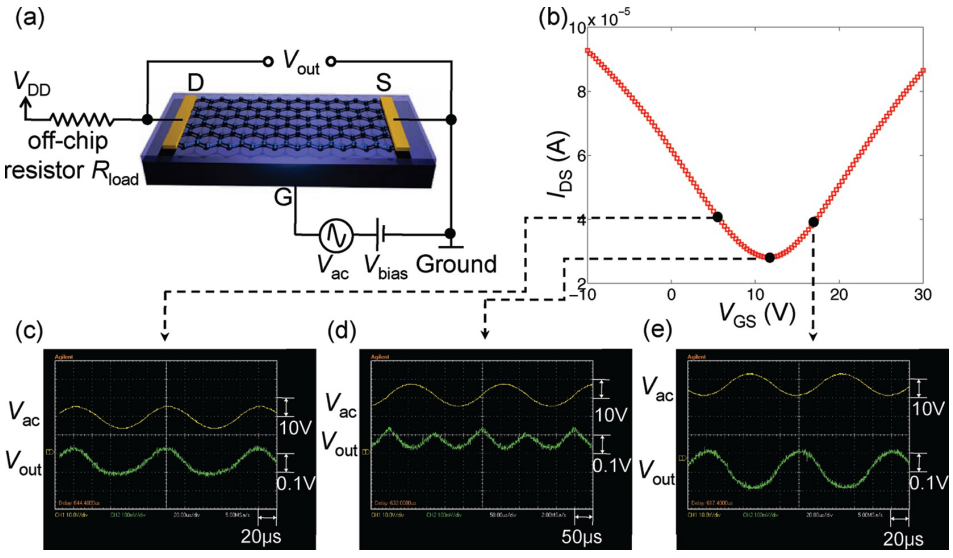

Figure 1.7: A GFET from [3]. (a) Schematic for the triple-mode single-transistor GFET. (b) The I-V characteristics of the GFET. (c) Input and output signals in the amplifier mode with 0° shift phase. (d) Input and output signals in the frequency multiplier mode. (e) Input and output signals in the amplifier mode with 180° shift phase.

- Analog electronics provide systems with a continuously variable signal. These systems are classified in, linear circuits, such as amplifiers or filters, and non-linear systems, such as power detectors, frequency multipliers or switches.

  Applications of GFET in the analog field are widely explored. In [44], authors provide a first attempt to explore the capabilities that GFET can provide and point out

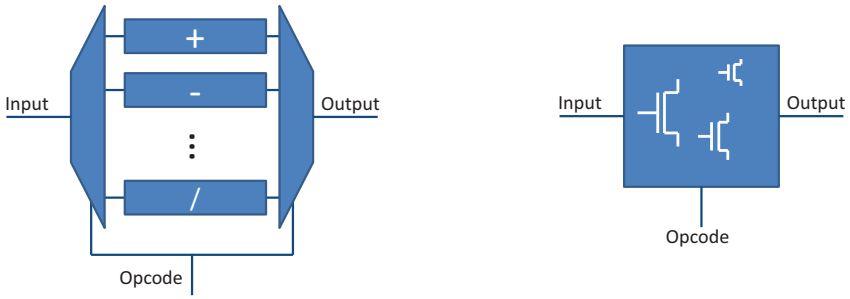

Figure 1.8: Expected evolution of digital systems for nanoscale applications. From using the opcode to select different functions to use the opcode to reconfigure the internal connections.

to the future development of amplifiers and frequency multipliers. Recently, authors in [45] validate for the first time that predictions. Their results show that the ambipolar properties of graphene transistors can configure the circuit to perform three different functions. As shown in Fig. 1.7, a single transistor can operate as an amplifier providing an output with the same frequency and phase or an amplifier providing the same frequency but shifting the phase 180º. Also, it can operate as a frequency multiplier. The frequency multiplier properties have been widely explored by Palacios *et al.* in [46].

Recent advances in manufacturing processes have enabled the integration of graphene circuits on a single silicon carbide wafer. Authors in [3] propose an integrated circuit that operates as a broadband radio-frequency mixer at frequencies up to 10 gigahertz.

- Digital electronics represent discrete and logical values by bands of analog levels. In this classification we find switching devices, such as logic gates, memories or processors. Graphene technology is providing graphene transistors in the nanoscale, reducing size and power and increasing the maximum switching frequencies [23, 24].

  Moreover, the ambipolarity of GFET is opening up new possibilities to achieve more complex functionality in the nanoscale. Similar to analog graphene devices, digital graphene technology is enabling multi-tasking logic gates. These new logic gates enables with a single graphene component the implementation of transistors that performs different logic functions according to the input levels [47, 48].

  These novel logic gates, not only can reduce the size and power consumption by using nanomaterials, but also, they allow to reconfigure the logic function in real time. Considering the reconfiguration of a large group of logic gates, a single unit can provide different responses according to the necessity in each moment. This paradigm dramatically reduce the size in current logical circuits. As shown in Fig 1.8, we expect that digital circuits will reduce their size by reconfiguring in real time the internal structure according to the operation code (*opcode*), rather than using the *opcode* to chose the function to use.

Terahertz sources

The Terahertz band is the band located between the microwaves and the far infrared, whose wavelength range is between 100-1000 μm (300 GHz - 3 THz). This band has the ability to penetrate several non-conducting materials and is defined as non-ionizing and then, it is not expected to damage tissue or DNA. For this, among other applications, the terahertz band has gained great interest in the recent years. However, up to now, the implementation of devices operating in the Terahertz band has been a great challenge and, for this, we barely know about channel characterization or performance at these frequencies.

Miniaturization provides high speed properties to the devices. This fact makes nanotechnology to be suitable for working with this novel band. Moreover, graphene based nanoelectronics set this band as the most suitable band for the implementation of nano-antennas and nano-transceivers. In [49], the analysis of a graphene nano-patch antenna is done showing that its operating frequency is in the terahertz band. Lin, Y. M. *et al.* envision in [50] operating frequencies in the order of terahertz for GFET in a near future.

However, the most difficult component to realize in the terahertz band is the Terahertz source. Currently, electronic oscillators up to gigahertz are low cost feasible. Optical sources, working at hundreds of Terahertz are also easy to implement. Terahertz sources presented up to now are optical and must operate at low temperatures (10 K - 30 K). These sources are limited by their low efficiency, and size and weight [51].

Furthermore, the generation of low-power, high efficiency, nano-power generators in the Terahertz band results more challenging. We consider that the main technologies that will satisfy these high technology requirements in the future are:

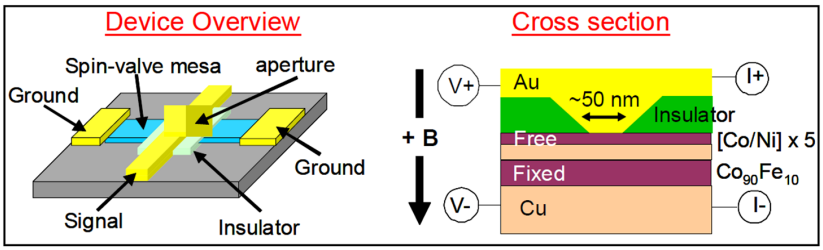

Figure 1.9: STNO device geometry

- *RF NEMS:* Nano Electro Mechanical Systems are devices that integrate electrical and mechanical functionality in the nanoscale, where both domains interfere to each other. The interaction between domains makes NEMS to be a suitable technology for the implementation of nano-sensors, where a mechanical effort can be transduced into a signal, for the implementation of energy harvesting systems, where a mechanical effort is transduced into electrical energy or for the implementation of actuators, where electrical energy is transduced into mechanical movement.

In [52], authors conclude their work expecting that using Graphene RF-NEMS, oscillation at frequencies beyond 1 Terahertz are possible. The use of this technology is very encouraging since it is manufactured with graphene technology. However, the transduction to the mechanical domain makes the device to be sensitive to changes in its close environment which will affect in its oscillation frequency, phase or spectral purity.

- *Spin Torque Nano-Oscillators:* Magnetic Spin Torque Nano-Ocillators (STNOs), shown in Fig. 1.9, are a radio frequency technology able to operate at low-voltage. These oscillators at the nanoscale are a promising low-voltage, room temperature, frequency agile, on-chip oscillators, sources or clocks. The theory of these nano-oscillators has been developed for several years [53], and in the recent years we can find several experiments and realizations [54, 55] where the STNO is able to generate power at frequencies in the range of 10-20 gigahertz. These experiments have been done with STNO of about 100 nm in diameter. However, in [54, 56], the STNO are expected to work at Terahertz frequencies as long as the device diameter could be reduced to 5 nm.

  However, up to now, these devices are affected by very low power efficiency. To mitigate this low efficiency, authors in [55] prove that this device has a phase-lock behavior when two or more STNO are connected in parallel increasing the spectral purity and power efficiency.

- *Upconverters:* Due to the lack of Terahertz oscillators, the use of upconverters to obtain Terahertz sources from Gigahertz oscillations is considered the most common technique. Several successful experiments have been done to prove this Terahertz signal generation. However, the results still show low efficiency and low spectral quality when the conversion ratio is above x4 [57]. However, all these experiments have been done for microtechnology, where the source finally is much greater than the nanomachine dimensions.

  For this, according to the work done in [46, 58], due to the non-linearities of GFET, graphene presents exceptional qualities, such as spectral purity or efficiency, in frequencies multipliers and, although, few experiments have been done and at low frequencies, T. Palacios envision GFET as a solution for high efficiency and high spectral purity which will allow not only the creation of Terahertz sources, but also in the nanoscale.

- *Plasmon:* This is defined as a quantum of plasma oscillation. In the same way that photons and phonons are quantization of light and mechanical vibrations, this plasmon is a quasi-particle resulting from the quantization of plasma oscillation. A plasmon is a collective oscillation of free electron gas density.

  F. Rana in [59] proposes and discusses coherent Terahertz sources on Plasmon amplification in 2D graphene. In this paper, the Plasmon gain to reach the oscillation is

analyzed and, due to the large gain values of graphene at Terahertz frequencies, this work could lead to integrated oscillators for electronic devices in the range of μm.

There are promising alternatives to generate the Terahertz sources for the digital clocks. However, up to now, the central frequency of the Terahertz power generated by these sources depends on the energy, current or environmental phenomena. The lack of stable crystal oscillators in the nanoscale will limit the performance and will condition the design frame to achieve synchronization between nodes and to guarantee the successful information exchange.

1.2.2 Terahertz Channel Modeling for Wireless Nanosensor Networks

In this section, we show how graphene nano-antennas set the Terahertz band as their resonant frequency. This property of nano-antennas is enough to propose the Terahertz band to enable the communication among nanodevices. Thus, we also show in this section a channel model for the Terahertz Band and we further introduce a simple modulation scheme based on the exchange of non-coherent femtosecond-long pulses spreads in time.

Graphene-based Nano-antennas for Terahertz Communications

Authors in [60], proposed the use of CNTs and GNRs to implement nano-dipole and nano-patch antennas. An schematic diagram of both antennas is shown in Fig. 1.10. The use of graphene to implement these nano-antennas is proposed to enable the integration of the antenna in the nanodevice, which is expected to be designed mainly using this technology.

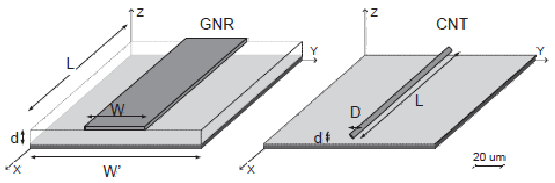

Figure 1.10: Nano-patch GNR antenna (left) and Nano-dipole CNT antenna (right) [2].

In [2], the authors analyzed the first resonant frequencies of a nano-dipole CNT-based antenna, whose length is set to 1 μm, this size was chosen to guarantee the integration of a nano-antenna inside a nanodevice. The results show that the first resonant frequencies of a nano-dipole are located in the Terahertz Band (from 0.1 THz to 10 THz) depending on the nanotube width and the energy used to feed the nanotube.

Fig. 1.11 shows the effect that the diameter of the nanotube has over the first resonant frequency and the transmission line resistance for different values of the energy used to feed the nanotube. As shown, an increase in the feeding energy or the nanotube diameter increases the first resonant frequency and reduces the resistance.

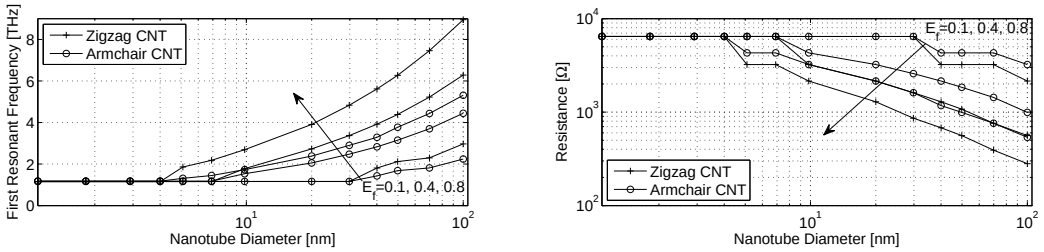

Figure 1.11: First resonant frequency (left) and Transmission Line Resistance (right) [2] .

The fact that graphene-based nano-antennas set the Terahertz Band as their frequency of operation opens up new possibilities and challenges. The Terahertz band is an unlicensed frequency band between the between the very high frequency microwaves and the far infrared that can provide a huge bandwidth. However, this band is one of the least explored frequency ranges in the EM spectrum.

Terahertz Channel Modeling: Path Loss and Molecular Noise

The Terahertz band has been widely explored in the imaging field. Terahertz imaging pursues a novel non-radiative alternative to radiography. The use of this technique covers several applications. Amongst others, Terahertz imaging is proposed, in the medical field, to detect infectious cancer tissue [61] and it is also proposed in security applications, such as metals or weapons detection [62].

For communication purposes, the Terahertz band is one of the least explored spectral ranges. As shown in the previous section, nano-antennas implemented in the future nanodevices will radiate in the Terahertz band. For this, in [4], the authors presented a novel propagation model based on *radiative transfer theory* [63]. This model describes the attenuation and noise that a Terahertz signal suffers when propagating through the medium composed by a percentage of water vapor molecules.

- Total Path Loss

  The still unlicensed Terahertz Band does not allocate services which can interfere with the proposed communication paradigm among nano-devices, but the resonance frequencies of some molecules has a strong effect the Terahertz channel. The molecule excitation of some molecules, such as water molecules, is produced throughout all the Terahertz band. This excitation attenuates the signal and introduces molecular noise.

  The propagation model in [4] copes with this effect by considering that when molecules are excited by waves with specific frequencies in the Terahertz Band, molecules absorb the energy carried by the wave and they transform a percentage of this energy into kinetic energy. This transformation is expressed by means of an EM loss in dB, $A_{abs}(f, d)$, and it can be described by:

$$A_{abs}(f, d) = -10log_{10}\left(\tau(f, d)\right) \tag{1.1}$$

where f stands for the frequency wave, d is the path length, and τ is the transmittance of the medium.

The transmittance can be related with the medium absorption coefficient, $k(f)$, by assuming that the medium is homogenous:

$$\tau(f,d) = e^{-k(f)d}. \tag{1.2}$$

The medium absorption coefficient, $k(f)$, does not depend on the distance, but on the medium composition, i.e., type of molecules, concentration, temperature, etc. This can be obtained from HITRAN (HIgh resolution TRANsmission molecular absorption) database [4].

Beside the molecular absorption, electromagnetical waves are also attenuated because of their expansion as long as they propagate through any medium, i.e., free-space loss. This attenuation is expressed in dB by:

$$A_{spread}(f,d) = 20log_{10}\left(\frac{4\pi fd}{c}\right) \tag{1.3}$$

where f stands for the wave frequency, d is the path length and c is the speed of light in the vacuum.

Finally, the total path loss or attenuation, $A(f,d)$, is expressed in dB as the addition of two attenuation terms, the spreading loss, $A_{spread}(f,d)$, and the absorption noise, $A_{abs}(f,d)$,

$$A(f,d) = A_{spread}(f,d) + A_{abs}(f,d). \tag{1.4}$$

- Molecular Noise

  The accumulated kinetic energy of molecules due to Terahertz excitation is re-radiated by molecules causing a background noise that affects the ongoing transmission. Therefore, the molecular absorption does not only attenuate the electromagnetic signal, but it also introduces noise. This phenomenon can be measured through the emissivity of the channel, ϵ, which follows:

  $$\epsilon(f,d) = 1 - \tau(f,d) \tag{1.5}$$

  where $\tau(f,d)$ is the transmissivity of the medium. Notice that the existence of molecular noise is directly related with the existence of a source which provides energy to these molecules. Therefore, if no source is radiating in the Terahertz Band, molecular noise does not exist.

  The equivalent noise temperature due to molecular absorption, $T_{mol}(f,d)$, in Kelvin that an omnidirectional antenna will detect from the medium can be obtained as:

  $$T_{mol}(f,d) = T_0\epsilon(f,d) \tag{1.6}$$

where T_0 is the reference temperature and $\epsilon(f, d)$ refers to the emissivity of the channel and depends on the frequency and distance.

Different resonances are generated by different vibrant molecules. We assume that frequency components are independent so each component can be modeled as Gaussian. The total noise power, P_n, for a given bandwidth, B, can be easily calculated as:

$$P_n(f, d) = \int_B k_B T_{mol}(f, d) df. \tag{1.7}$$

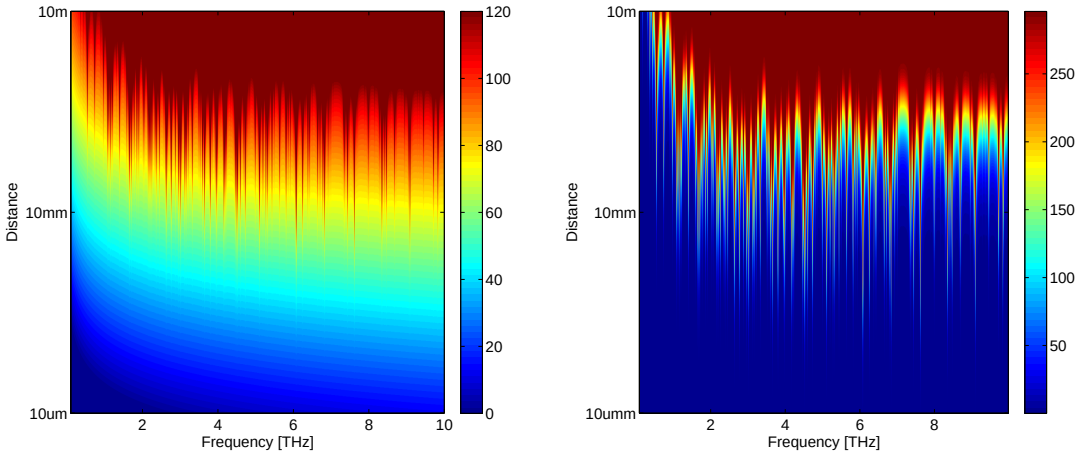

Figure 1.12: Total Path Loss in dB (left) and Noise Temperature in K (right) for 10% of H_2O [4].

Fig. 1.12 shows the Total Path Loss in dB and the Noise Temperature in Kelvin as function of path length and frequency. While the frequency axis is spread along the whole Terahertz Band, the distance axis just goes from some tenths of micrometers to some tenths of meters. This distance and frequency relation entails to choose between two types of communications in the Terahertz Band. Either broadband short range communication (up to few mm) or narrowband communications with larger ranges (up to few m) in the sub-Terahertz bandwidths. Transmitting simultaneously at different frequency windows requires multi-radio, complex transceivers capable of it, while broadband communications can simplify the transceiver architecture. Therefore, we envision the communication among nanodevices to be feasible in the short range, using broadband modulations and occupying the whole Terahertz Band.

1.2.3 TS-OOK: Time-Spread On-Off Keying Mechanism. Pulse-Based Communications

The Time Spread On-Off Keying (TS-OOK) modulation scheme is based on the transmission of femtosecond-long symbols spread in time. These symbols are pulses or silences according to an On-Off Keying modulation. TS-OOK is a particular case of pulse-based communications. The use of pulse-based communications removes the use of high

The Time Spread On-Off Keying (TS-OOK) modulation scheme looks at the Terahertz Band as a single transmission window almost 10 THz wide. In consequence, the transmission range under this scheme is bound to the short range (just up to few mm). TS-OOK is based on the transmission of femtosecond-long symbols —pulses or silences (On-Off Keying)— spread in time (Time Spread).

On the one hand, the On-Off keying modulation is chosen instead of other more efficient modulations (Pulse Amplitude Modulation (PAM) or Pulse Position Modulation (PPM)) because of two reasons. First, the simplicity of this modulation allows the use of a basic energy detector to demodulate the information at the receiver side. Second, the molecular absorption in the Terahertz Band entails a noise-free transmission channel when transmitting silences. This peculiarity can be widely exploited by codification schemes in the Terahertz Band that transmit more silences than pulses [64].

On the other hand, the spreading factor responses to different physical reasons such as device constraints, channel multi-path or energy scarceness. The device limitations for which nano-devices might not be able to process input data at high symbol rates —$1/T_p \approx 10^{12}$ $[symbols/sec]$—, but they will at slower symbol rates —$1/\beta T_p \approx 10^9$ $[symbols/sec]$— depending on a spreading factor β. Moreover, causal multipath will also affect the transmitted signal by creating several delayed versions of each femtosecond-long pulse. The spreading will also alleviate the multipath effect over consecutive symbols of the same signal, eliminating the Inter Symbol Interference (ISI) of this paradigm. Finally, the spreading also responds to the lack of energy in nano-devices. By spreading symbols in time, we allow nano-devices to have more time to harvest energy from the surroundings.

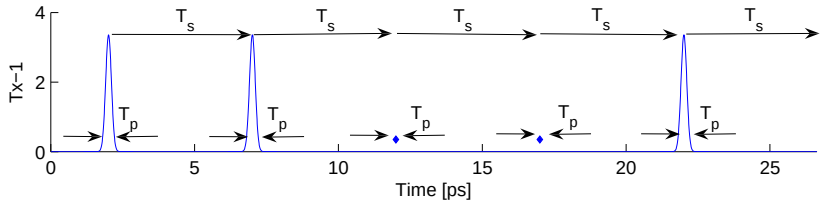

Figure 1.13: Transmitted Time Spread On-Off Keying (TS-OOK) signal for a given user.

Fig. 1.13 shows the transmitted TS-OOK signal for a given user. The figure is scaled accordingly to properly represent the information on it. Typically, we envision a time between symbols, T_s, to be thousands of times bigger than the symbol width T_p. The TS-OOK signal can mathematically be represented by:

$$s_T(t) = \sum_{k=1}^{N_s} A_k p(t - kT_s - \tau) \tag{1.8}$$

where N_s is the number of symbols per packet, A_k refers to the amplitude of each transmitted symbol, $p(t)$ is a T_p-width Gaussian pulse, T_s stands for the time between symbols and τ is a random delay that indicates the asynchronicity of the node.

The transmitted TS-OOK signal is then propagated through the Terahertz channel. Considering the propagation model introduce in Section 1.2.2, the signal at the receiver side can be expressed by means of the channel impulse response, $h^R(t)$, and the Additive Gaussian molecular noise, $w_k^R(t)$:

$$s_R(t) = \sum_{k=1}^{N_s} A_k p(t - kT_s - \tau) * h^R(t) + w_k^R(t). \tag{1.9}$$

TS-OOK Single-user Information Capacity

The channel capacity of the Terahertz Band was analyzed and studied in [4]. The results state the expected high capacities for any power spectral density (p.s.d.) allocated in the whole THz band. Moreover, the analytical results also point at the transmission of femtosecond-long pulses would perform in terms of capacity closed to the capacity-optimal p.s.d..

However, the channel capacity analysis does not consider the effects of the pulse-based modulation on top, and the capacity results are not closed to the realistic data rates for nano-devices. With the aim of achieving the single-user information capacity, the authors in [65] propose a way to estimate the user capacity, C_u, from the well-known Shanon limit theorem:

$$C_u = \frac{B}{\beta} \max_X I(X,Y) = \max_X \; H(X) - H(X|Y) \tag{1.10}$$

where X refers to the source information, Y refers to the output of the channel, $H(X)$ is the entropy of the source, $H(X|Y)$ is the conditional entropy of X given Y, commonly referred as channel equivocation; B is the signal bandwidth and β is the ratio between time between symbols, T_s, and pulse width, T_p.

Based on the statistical molecular noise model proposed in [65], the noise can be modeled as an additive Gaussian noise with mean equal to zero and variance given by the addition of the noise power corresponding to each resonance $\mathcal{N}(\mu = 0, \sigma^2 = \sum_v \sigma_v^2)$. Provide this statistical molecular noise model, equation (1.10) can be rewritten in terms of the symbol probabilities $p_X(x_m)$, the received symbol amplitude, a_m, and the total noise power, N_m:

$$\begin{aligned} C_u \; = \frac{B}{\beta} \max_X \{ & - \sum_{m=0}^{1} p_X(x_m) \log_2 p_X(x_m) - \int \sum_{m=0}^{1} \frac{1}{\sqrt{2\pi N_m}} e^{-\frac{1}{2}\frac{(y-a_m)^2}{N_m}} p_X(x_m) \\ & \log_2 \left(\sum_{n=0}^{1} \frac{p_X(x_n)}{p_X(x_m)} \sqrt{\frac{N_m}{N_n}} e^{-\frac{1}{2}\frac{(y-a_m)^2}{N_m} + \frac{1}{2}\frac{(y-a_n)^2}{N_n}} dy \right) \} [bps] \end{aligned} \tag{1.11}$$

Fig. 1.14 shows the single-user capacity described by equation (1.11) as a function of distance for different levels of background noise, N_0. The behavior of the capacity with distance is very peculiar. First, for distances below few millimeters, the capacity is almost constant and equal to $1 bit/symbol$. Then, as the distance increases, the capacity abruptly fall to lower capacity values depending on the background noise. The distance for which the capacity falls down is given when the received signal and the noise power become close in

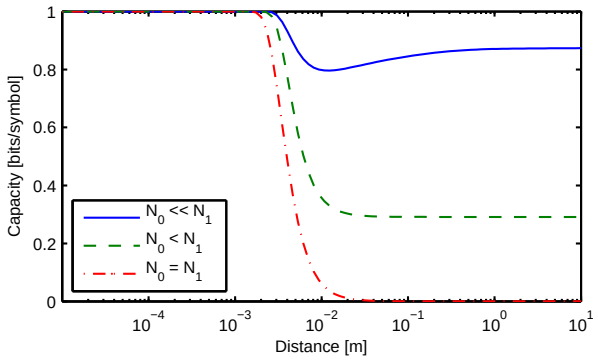

Figure 1.14: Single-user capacity as a function of distance in bits/symbol for different levels of background noise, N_0. [5]

magnitude. Finally, If the level of molecular noise, N_1, is much bigger than the background noise, the capacity increases again up to a limit. This increase is due to the molecular noise created by the pulse propagation, permits better differentiation between symbols at the receiver side.

However, the aforementioned capacities are constrained to the receiver scheme used. In the next section, we focus on analyzing the pros and cons of two possible transceiver designs: *coherent* and *non-coherent* receivers. However, non-coherent designs are much simpler to be implemented in nano-devices and hence we study their performance more deeply in terms of Symbol Error Rate (SER). Regarding the non-coherent design, we also propose a low complexity multi-user scheme capable of demodulating up to k concurrent users.

1.2.4 Enegrgy Constraints in Electromagnetic Nanonetworks

In the nanoscale, the power management is expected to be one of the main challenges in the nanonetworks paradigm. However, the expected size reduction of each and every one of the blocks implicitly implies a power reduction in several orders of magnitude. Self-Powered Nanodevices stands for these nanodevices which are capable of absorbing the available energy in their close environment and use it to supply their internal circuits. These concepts pursue the recently introduced *Zero-Power* ICT and *Perpetual* operation.

The expected energy sources to supply these nanodevices can be found in their close environment. Amongst others, we can extract energy from acoustic waves, temperature variations, solar energy but mostly vibrations. As an example, recent developments in ZnO nanowires proved that these nanowires are able to generate electrical power if these are streched [30]. This technology is expected to provide a framework to support the perpetual operation in nanosensor networks, by connecting hundreds of nanowires in the base of the nanodevice (See Fig. 1.1).

The energy sources available in the nanoscale, although ubiquitous, present an erratic behavior in time and frequency. This fact means that the nanodevice cannot guarantee that

there is always available energy to enable its operation. For this, we envision that a capacitor will be included to store the available energy when there is more energy harvested than used and to provide the necessary energy when the harvested is not enough to supply the overall operation. In particular, Onion-Like-Carbon (OLC) capacitors have been explored in [28]. These capacitors support very fast charging and discharging rates and well behave in front of pulsed energy fluctuations.

The size constraints (10 - 100 μm^2) of these nanodevices makes the maximum storage energy inside the capacitor to be around some hundreds of picojoules, which is comparable to the needed energy to transmit a few packets. Additionally, the available energy that a nanodevice of these dimensions can harvest is limited to some picowatts.

This context makes that the nanodevice can generate and transmit a very few packets of a few hundreds of bits length per minute. Sending a packet of a few hundreds of bits using the TS-OOK modulation scheme takes in the order of a few tens of nanoseconds. This is nine orders of magnitude below the packet generation rate.

Thus, the energy limitations in WNSNs will present high limitation in the development of novel nanodevices and design of novel transceiver for nanonetworks and it presents several challenges in the synchronization among nanodevices, since a synchronization error of some nanoseconds is comparable to the packet length.

1.3 Motivation and Contributions

The communications alternatives for nanodevices are still very limited. Amongst others, graphene-based RF nano-components [59] and graphene-based nano-antennas [60] set the Terahertz band (0.1 - 10.0 THz) as the expected frequency range of operation for the future EM nano-transceivers. This band is one of the least explored frequency ranges in the EM spectrum, in between the very high frequency microwaves and the far infrared.

As the authors in [4] showed, on the one hand, the Terahertz band provides a huge bandwidth in the short range that can support very high transmission rates, up to hundreds of terabits per second. On the other hand, this huge bandwidth can also enable simple modulations which relax the nano-transceiver requirements. As shown in [66], very short pulses, just one hundred femtosecond long, can be efficiently generated and radiated without the need of high frequency sources. These pulses have their main frequency components in the Terahertz band and thus can be efficiently radiated using wideband Terahertz nano-antennas. This fact enables the use of femtosecond-long impulse-based modulations. As an example, the Time Spread On Off Keying (TS-OOK) has been recently proposed in [64]. This modulation is based on the asynchronous exchange of femtosecond-long pulses following an On-Off scheme.

In this context we propose to define the bridge between the nanodevice and the nano-antenna. First of all, we propose a novel transceiver architecture specially designed for

pulse-based communications. Its transmitter converts the logical information provided by the nanodevice to electrical voltages to supply the antenna. This transmitter modulates the signal using femtosecond-long pulses spread in time. Its receiver demodulates the signal using a variation of the classic power detection scheme implemented with a continuous-time integrator which improves the performance in terms of symbol error rate for pulse-based modulation schemes.

The n

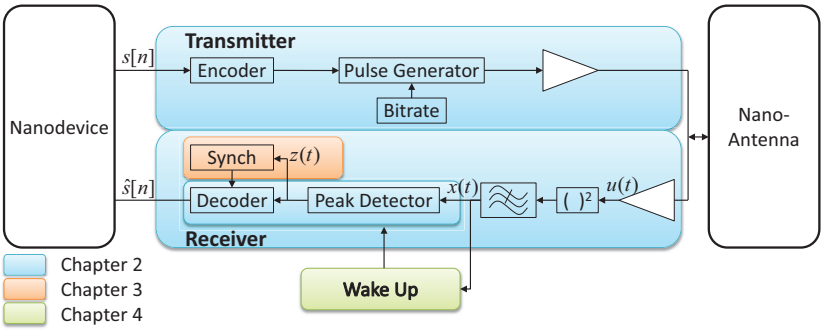

Figure 1.15: Block diagram of the main contributions in this work. In the Chapter 2 we propose the transceiver architecture, in chapter 3 we propose a symbol time estimator and in chapter 3 we propose an asynchronous synchronization scheme based on a remote wake-up receiver.

on-idealities observed in Terahertz sources leads to consider the effects of frequency drifts in the reception of of information from a neighboring nanodevice. These frequency drifts between the transmitter and receiver nanodevice oblige to perform a symbol time estimation before any transmission is started. For this, we also propose a symbol time estimation scheme built on top of the transmitter architecture proposed. We propose a simple mechanism to synchronize frequencies and we explore the effect of this estimation over the packet error rate estimation.

Up to this point, two nanodevices are able to communicate each other. They are capable of correctly detecting the upcoming symbols and to correct any possible frequency drift among them. However, as shown in Sec. 1.2.4, the energy constrains in the nanoscale makes this nanodevices to generate very low traffic and transmit their information spread in time. Additionally, unlike typical WSN, these are strictly based on Self-Powered concepts which consider the nanodevice OFF state due to energy depletion as, not only possible, but frequent state. This OFF state implies that nanodevices are frequently losing any existing synchronization.

This particular situation of nanonetworks disables classical duty cycled synchronization schemes and motivates the research on asynchronous synchronization schemes for nanodevices. In this work, we propose an asynchronous synchronization scheme based on a wake-up receiver, where the transmitter remotely wakes up the receiver before the transmission. We discuss the effects that this novel scheme has over the needed energy to receive and decode a packet, as well as the probability of detecting upcoming packets.

Fig. 1.15 locates these three main contributions into the nanodevice architecture.

1.4 Structure

The rest of this work is organized as follows. In Chapter 2, we present the transceiver architecture scheme and evaluate its performance. In Chapter 3, we present the effect of the non-idealities over the reception of packets and we propose a symbol time synchronization scheme to successfully decode the information. In Chapter 4, we present an asynchronous synchronization scheme to detect new transmission of packets based on a wake-up receiver. Finally in Chapter 5, we conclude our work.

Chapter 2

A Transceiver Architecture for Electromagnetic Nanonetworks in the Terahertz Band

2.1 Introduction

The Terahertz band provides a huge bandwidth in the short range that can support very high transmission rates, up to hundreds of terabits per second. However, this huge bandwidth can also enable simple modulations which relax the nano-transceiver requirements and simplifies the communication among nanodevices. As shown in [66], very short pulses, just one hundred femtosecond-long, can be efficiently generated and radiated without the need of high frequency sources. These pulses have their main frequency components in the Terahertz band and thus can be efficiently radiated using wideband Terahertz nano-antennas. This fact enables the use of femtosecond-long impulse-based modulations. As an example, the Time Spread On-Off Keying (TS-OOK) has been recently proposed in [64]. This modulation is based on the asynchronous exchange of femtosecond-long pulses, spread in time, following an On-Off scheme (Logical "0" are transmitted as silence and logical "1" as pulses).

Novel transceiver architectures for nanonetworks must be proposed to support the operation of TS-OOK, and any other type of femtosecond-long pulse based communication scheme. These transceiver architectures must be based on high simplicity. Existing receiver architectures for pulse-based communications, such as Impulse Radio Ultra-Wide-Band (IR-UWB) [67], consist of a classical non-coherent receiver architecture, where the input signal is integrated over a time window after a power detection. While this receiver architecture provides very good results in terms of energy efficiency when the time window is as short as the pulse width, the existing clock drifts, highly influenced by this time-spread, carrierless modulation, among nanodevices force this time window to be increased in 10 to 100

times. This effect drops the performance in terms of signal to noise ratio, SER and channel orthogonality.

In this context, we propose a novel transceiver architecture for nanonetworks designed to support the operation of TS-OOK, and any other type of femtosecond-long pulse based communication scheme. This transceiver architecture copes with the peculiarities of non-coherent pulse-based modulations, focusing on the Terahertz band. The main novelty of the proposed architecture is in the symbol detection. This is based on a *continuous-time* detection scheme. In particular this symbol detector seeks for the maximum during a time interval previously defined and compares this maximum with the established threshold. As we show in the results, this scheme outperforms existing receiver architectures [67, 68, 69] in terms of simplicity and robustness, which are mainly based on an *integration and sampling* approach.

The main contributions of this chapter can be summarized as follows:

- We propose a novel transceiver architecture for EM nanonetworks, based on a continuous-time detection scheme.
- We develop an analytical model for the symbol detection probability and investigate the impact of different parameters on the symbol error rate.
- We develop a post-simulation model to simplify the estimation of the symbol receiver SER and we explore the impact that the inter symbol interference (ISI) has over the maximum achievable bitrate.

The rest of this chapter is organized as follows. In Sec. 2.2, we describe the new transceiver architecture. In Sec. 2.3 we describe the symbol detection mechanism and we develop an analytical model to estimate its symbol error rate. In Sec. 2.5 we validate the model and evaluate the performance of the receiver. In Sec. 2.6 we conclude the work presented in this chapter.

2.2 Transceiver

In order to provide the successful communication among nanodevices, we propose a novel transceiver architecture to support femtosecond-long impulse-based modulations, such as TS-OOK. The transceiver block diagram is shown in Fig. 2.1, where $s[n]$ refers to the input data stream to be transmitted and $\hat{s}[n]$ the output data stream received from the channel. We next describe each of the blocks of the transceiver architecture. Note that we do not specify any concrete technology for these blocks, although graphene technology is expected to provide a framework for the design of each block proposed [44, 47, 48], but the novelty of this transceiver is on the architecture itself.

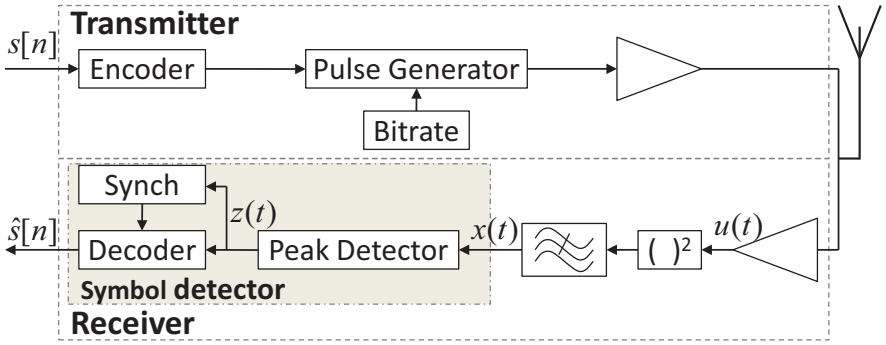

Figure 2.1: Transceiver Block diagram Architecture

2.2.1 Transmitter Architecture

We propose an All-Digital transmitter architecture to reduce the overall energy consumption of the transmitter. This transmitter avoids the use of a high frequency source to feed the antenna by generating the output signal from a combination of very short pulses generated with logic gates. The reduction of this high frequency source is highly recommended in low-power impulse-based transceivers. These sources require high power requirements that can dramatically increase the power consumption and disable any chance of developing communication-enabled nanodevices in the near future.

This concept of All-Digital transmitter has been introduced in current communication schemes, such as IR-UWB [70, 71], because by avoiding the use of high frequency sources the energy/bit is reduced. In TS-OOK, this implementation receives much more strength since the signal transmitted is just a single pulse, while in other communication schemes, such as IR-UWB, the pulse is composed by the addition of tens of oscillations. As shown in Fig. 2.1, the transmitter part of the transceiver consists of:

Encoder

The binary data that needs to be transmitted is sent to the transmitter block as logical values. The first thing the transmitter must do is to encode this data, if any codification is being used and to provide this output data to the transmitter to be modulated. In [64], we provided a codification scheme to mitigate the interference among nanodevices. If there is no codification, this block just provides a memory, or buffer, to store the data until it is sent. Additionally, if MAC protocols are designed on top, this memory should also keep the data, not until the data is sent, but until the data is successfully sent or discarded. The use of buffers or memories is encouraged to release the nano-processing unit from the control of the transmission.

Pulse Generator

The conversion digital to analog is done in this block. Using All-Digital systems, the symbol is converted to a 100 femtosecond-long pulse if the symbol is a logical "1" or to silence if it is a logical "0". The timing for the 100 femtosecond-long pulse is provided by this block. Every time a new symbol period T_s starts, the All-Digital pulse generator converts this symbol into a femtosecond-long pulse. To generate only one short pulse, around a thousand times shorter than the symbol period, we envision the use of differentiator circuits. The timing to generate the symbol time, T_s is provided by the Bitrate block.

Bitrate

This block provides the bitrate, defined as $R = 1/T_s$, for the transmission. This block can be designed using a basic binary counter. The use of digital counters instead of analog timing schemes has two main benefits: On the one hand, digital circuits decrease the power consumption and provides an elevated accuracy in this timing, while on the other hand, the use of digital circuits also provides the possibility of self-configurable bitrates for nanodevices. These self-configurable bitrate opens up a great deal of new possibilities. As an example, in [72], a physical layer aware MAC protocol was proposed for EM nanonetworks, using a rate division scheme to avoid catastrophic collisions.

Output Amplifier

A power stage is needed before feeding the nano-antenna. In this case we envision that this output amplifier is mainly composed by two components.

Firstly, as seen in Sec. 1.2.2, graphene-based nano-antennas are expected to modify their radiation profile according to their feeding energy. This is, nano-antennas modify their first resonant frequency and their antenna resistance. For this reason, we first need a power amplifier to fix the feeding energy in the antenna in the desired operating point. Additionally, the output can also be tunable to reduce the energy consumption in case the target nanodevice is in its close environment.

Secondly, to maximize the power transfer, the transceiver's output impedance must match with the antenna's input impedance. Thus, a matching network is needed to optimize the power transfer and increase the efficiency.

2.2.2 Receiver Architecture

In TS-OOK, very short pulses are spread in time at a constant rate $R = 1/T_s$. For this, the receiver can be switched off during the reception and just wake it up every T_s for a very short period of time, up to one thousand times shorter. Because of this short-time pulses, exact

synchronization between nanodevices is hard to achieve. To provide robustness in reception, this asynchronous receiver is proposed where the sampling stage is done after a continuous-time threshold comparator. With this, the novel architecture solves the problem of splitting the pulse into two different integration periods, spreading the total amount of energy and, also, it enables the sampling among consecutive time intervals. The receiver architecture is shown in Fig. 2.1 and consists of:

Terahertz Front-End

This is the dual block to the output amplifier block described in the transmitter. The Terahertz Front-End consists mainly of two blocks: First of all, An input filter is needed to reduce noise and match the antenna with the receiver architecture. This matching network will also transfer the maximum amount of energy to the following stages. The fact that the modulation uses a huge bandwidth allows the input filter to be designed using low-quality filters. Then, an amplifier is needed to condition the signal and to provide the enough voltage levels to be processed by the receiver.

Power Detector

A power detection is used for simplicity. Power detection means to calculate the input power from the input signal, this power detection is proportional to the function $(\ )^2$. The power detection is widely implemented in communication and other electronic systems and its implementation is very simple. Using different technologies, power detectors have been proposed with the use of diodes or transistors. We foresee that GFET technology will also provide a framework for the implementation of this power detector. The simplicity of non-coherent communication systems conducts to up to 10x power consumption savings in UWB systems [73]. Though these energy tests have not been performed for the TS-OOK modulation in the Terahertz band yet, we envision the non-coherent receivers with energy detectors will provide the best solution in the Terahertz band, as well.

Low-Pass filtering

After the power detector, we need a continuous-time integrator. We define a continuous-time integrator as the continuous version of the discrete function *moving average*. This is a linear time-invariant function given by:

$$y(t) = \int_{t-T}^{t} x(\tau) d\tau \tag{2.1}$$

There is no real system that can accomplish this function. For this reason, we propose the use of a second order low-pass filter with two real poles at the same frequency. This filter could

be easily implemented with a chain of two RC filters in cascade with orders of magnitude of R $\sim$ kΩ and C $\sim$ fF, or even solutions implemented with GFET, since their model implicitly includes a resistor and a capacitor [47] and provide a low-pass behavior. This low-pass filter, with impulse response $h_{lpf}(t)$ provides an approximation to the continuous-time integrator needed for the receiver architecture, characterized by its impulse response $h_{int}(t)$.

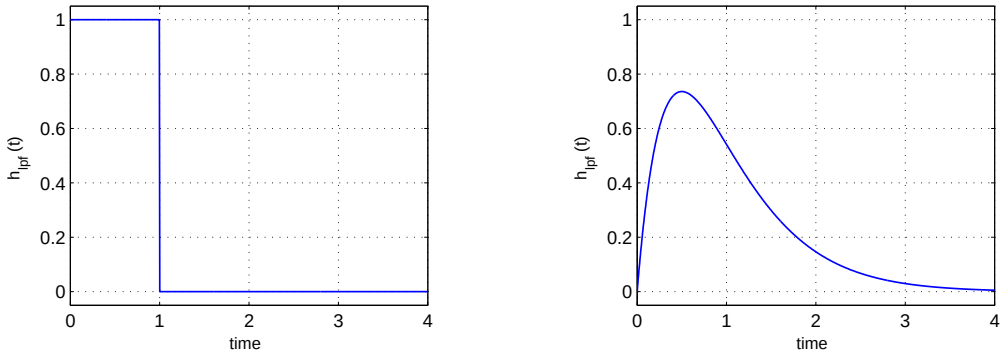

Figure 2.2: Impulse response comparison (out of scale) between the ideal integrator, $h_{int}(t)$, (left) and a second low-pass filter, $h_{lpf}(t)$, (right).

To determine the cutoff frequency or, equivalently, the time width of the low-pass filter, we propose a square error minimization between both impulse responses as function of the a parameter in $h_{lpf}(t)$ and T_p in $h_{int}(t)$. Then given the impulse responses:

$$h_{int}(t) = \begin{cases} \frac{1}{T_p} & \text{If } 0 < t < T_p \\ 0 & \text{Otherwise} \end{cases} \quad , \quad h_{lpf}(t) = a^2 t e^{-at} \tag{2.2}$$

where h_{int} is the impulse response of an ideal integrator with T_p time of integration and h_{lpf} refers to the impulse response of a second order low-pass filter with two real poles with parameter a.

In order to find the closer low-pass filter to the ideal integrator, we have minimized the square error between both impulse responses as function of the parameter a. This minimization gives that the relation between the parameter a of the second order low-pass filter and the pulse time T_p is $a = 1.4615/T_p$.

Peak detector

The proposed peak detector is based in continuous-time comparison. This is integrated by a comparator and a latch circuit that, whenever the input is higher than the threshold predefined, the output of the circuit is fixed to "1" until an external control circuit resets the output to "0". This is explained with more detail in Sec. 2.3

Synchronization

Since we have an output stream from the symbol detector, we must read the output in time to decode the packet. The synchronization block takes care of estimating the time between symbols and the time interval where the pulse can arrive. Then, it switches off the receiver until the next pulse is about to come. This synchronization block can also make the decoder to check the output several times during this time interval. If so, notice that the time resolution can be higher than the time interval, and then, can simplify synchronization schemes built on top. In what follows, we consider this block as ideal, so the pulse is always supposed to appear inside the time interval. The symbol time estimation is described in the next chapter, evaluating the effect that non-idealities has over the performance of the receiver.

Decoder

The decoder checks the output of the peak detector after the synchronization block decides the end of the time interval. This block takes care of translating the physical magnitude measured in the output of the peak detector into logical values. These logical values are stored in a memory and sent to the nanodevice in case the transmission is successful. Additionally, if the encoder was providing any codification scheme to protect the data, the decoder provides its inverse function.

2.3 Symbol Detection

The symbol detector presented in this paper consists of a peak detector, a decision maker implemented in the decoder and a sampler provided by the synchronization block. If at any instant of time, the input at the peak detector is above a prefixed threshold, its output is fixed to "1" until an external circuit resets it, otherwise is kept as zero. The synchronization block takes care of enabling the whole symbol detector when the new pulse is about to come and after a predefined time T, it makes the decoder block to check if a new pulse has arrived. As an example, Fig. 2.3 shows the symbol detection mechanism, where the signal $x(t)$ (See Fig. 2.1) is the output of the low-pass filter, $z(t)$ refers to the output of the peak detector and $\hat{s}[n]$ stands for the symbol decoded. Additionally, we show the signal $synch(t)$ which represents when the synchronization block enables / disables the receiver. As shown, $z(t)$ only turns to "1" when the enabling signal $synch(t)$ is activated. When the receiver is enabled, if a new pulse arrives, $z(t)$ is fixed to "1" until the synchronization block deactivates the receiver. At this moment, the decoder reads its input and decides the logic value ("0" or "1"). Finally, as the channel is shared with other nanodevices and applications, the receiver must be kept in standby until a new pulse is arriving. As shown, the interfering pulses that are arriving to the receiver are not decoded, since the synchronization block is disabling the receiver.

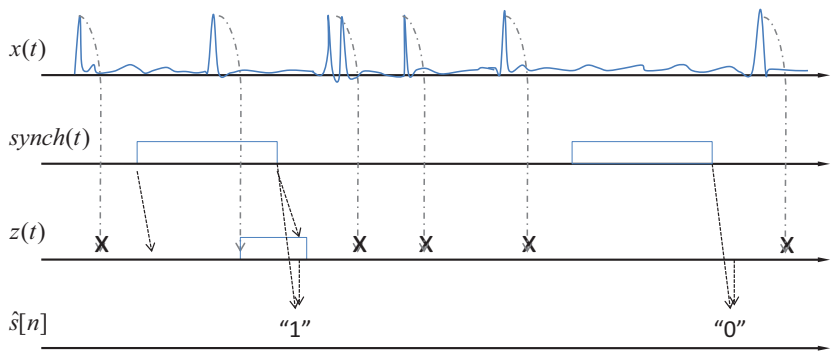

Figure 2.3: Example of signal values in the receiver architecture, during the reception of a logical "1" and a "0".

Usual symbol detectors sample the output of the integration or low-pass filtering in a single and predefined instant of time. In particular, in optical schemes [74], the symbol reception is phase synchronized using Phase Locked Loop (PLL) circuits and then the output is sampled in the optimal point. This detection is widely implemented in communication systems without time-spreading. In contrast, in time-spread carrierless communications, such as IR-UWB [67], the power is integrated over a time window and sampled at the end of this window. This case needs of high synchronization between devices before the transmission starts. To relax the synchronization constraints, in IR-UWB the integration time window is increased in the order of 10 to 100 time the pulse time, so they can make sure the pulse will arrive in this time. This increase of time makes the signal to be weighted with 10 to 100 times more noise than needed. This solution drops the performance of the receiver.

2.3.1 Continuous-time Symbol Detector

The main difference between this detector and previous detectors lies in the instant of time of detection. Usual detectors sample the input, $x(t)$ (see Fig. 2.1), in a predefined time instant and check if it is above or below the threshold.

The proposed detector checks if the signal $x(t)$ is above or below the threshold. If the signal is above the threshold, $z(t)$ is set to "1" until the end of the time interval. Finally, it samples the output $z(t)$ after a predefined time. This can also be interpreted as detecting a "1" if the maximum of the signal $x(t)$ during the defined time is above the threshold, otherwise it is detected as "0". When the observation time is large, this maximum function provides more distance between logical "0"s and "1" than the integration or average. Using this max function, we can express the decoded signal $\hat{s}[n]$ as:

$$\hat{s}[n] = \begin{cases} 1 & \text{if } \max\limits_{t\in(0,T)} x(t) > V_{th} \\ 0 & \text{otherwise} \end{cases} \tag{2.3}$$

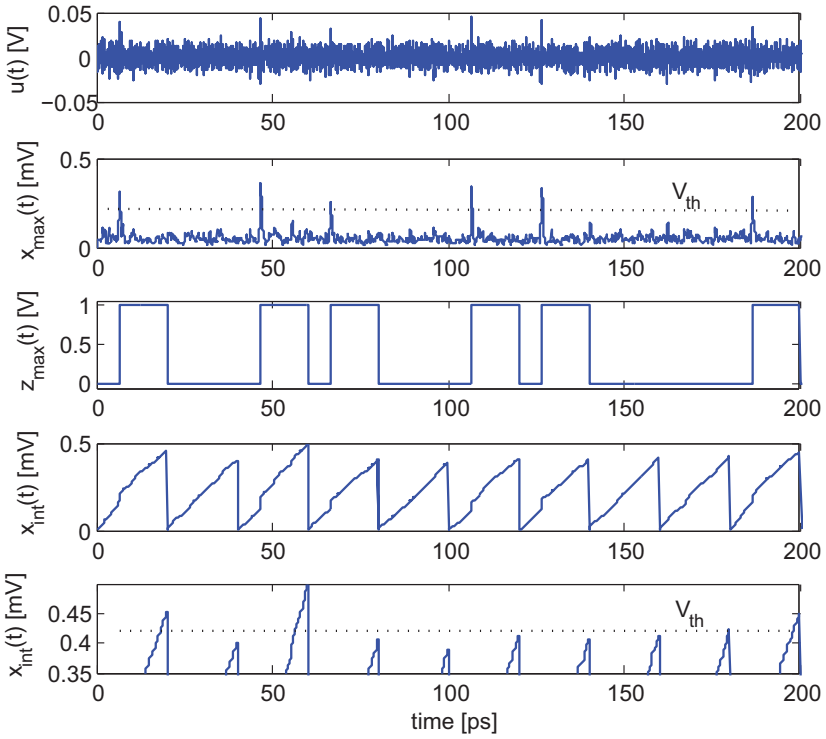

Figure 2.4: Comparison between the input signals at the symbol detector proposed and the current symbols detectors based on integration

where $x(t)$ is the input signal in the comparing threshold, T refers to the time of observation, and V_{th} is the threshold. This threshold is chosen to optimize the SER.

Authors in [67, 68] set the integration time for the pulse in the order of 15 times the pulse time due to the high limitations that usual receivers present when very short pulses spread in time are received, in terms of technology and symbol synchronization. This fact makes that each pulse is being averaged with around 15 times more noise energy than needed. To provide a better performance and a good trade-off in energy for the usual detectors, we propose this novel receiver that compares the maximum of the filtered signal during a time interval instead of averaging the signal with noise in the whole time interval. Then, as the time interval increases, this novel receiver provides a better output response. However if the time during the channel observation is reduced, both receivers tend to the ideal receiver because in the limit, the maximum of a single discrete variable is the variable itself.

Fig. 2.4 shows an example for the case in which the sequence "1011011001" is transmitted. $u(t)$ is the input signal, $x_{max}(t)$ stands for the input provided to the peak detector, the output of the peak detector is $z_{max}(t)$ where, as can be seen, holds the value until the sample instant of time, and the input to a current symbol detector $x_{int}(t)$ and a magnified view of this to observe the distance between symbols. As can be seen, for the same energy per bit and noise level, the distance between the signal and the noise is much greater allowing to our receiver to decode correctly the sequence, whereas in current detectors the sequence detected is "1010000011".

The fact that there is no integration in the symbol detector, makes that there are no dead zones where the pulse cannot be successfully received due to the fact that the pulse is split into two different time intervals. This fact makes that the time interval, T, can be adaptively modified during the reception, two time intervals, T, can be put one next to the other or even oversample this interval. These options leads to symbol time synchronization schemes that can allow the receiver to easily simplify the detection of the upcoming pulses. Symbol time synchronization is further explored in the next chapter.

2.4 Analytical Model for the Symbol Detection

The output of the Low-pass filter, $x(t)$, can be written for a single pulse arriving in a random time τ:

$$x(t) = \left(s[i]w(t - iT_s - \tau) * h_c(t) + n(t) \right)^2 * h_{lpf} \tag{2.4}$$

where $*$ denotes convolution, $s[i]$ stands for the transmitted symbol, that can be "0" or "1", $w(t)$ refers the 100 femtosecond-long pulse, T_s is the symbol period, $h_c(t)$ stands for the transfer function provided by the channel, $n(t)$ refers to the noise of bandwidth W and $h_{lpf}(t)$ is the impulse response of the low-pass filter. Then $\hat{s}$ is decoded according to (2.3).

To model $\max x(t)$, we consider that the SER tends to the ideal energy detector receiver when the time of observation tends to zero. This assumption is correct in case of using a continuous-time integrator. The use of a second-order low-pass filter will add an error when the time interval, T, is close to the pulse time, T_p. The low-pass filter, or continuous-time integrator, provides a high correlation between consecutive instants of time that enables the discretization of the continuous-time function $x(t)$ into N independent random variables. The number N of random variables is proportional to the time interval T.

With this, the function $\max x(t)$ can be expressed as function of the vector $\boldsymbol{X} = \{X_1, X_2, \cdots, X_N\}$ which refers to the discretized function $x(t)$ with:

$$\max_{t\in(0,T)} x(t) = \max_{N} \boldsymbol{X} = \max_{N} \{x(t_1), x(t_2), \cdots, x(t_N)\} \tag{2.5}$$

where T refers to the time of observation, N stands for the number of independent discretized variables, $x(t_1), \cdots, x(t_N)$ the value of the input signal $x(t)$ in the instants $t_1, \cdots, t_N$.

For the further calculation of probability density functions, we know that the given a set of independent random variables $X_1, X_2, \cdots, X_N$, with probability density functions $f_1, f_2, \cdots, f_n$ and cumulative distribution functions $F_1, F_2, \cdots, F_n$, we can express the maximum among these variables in terms of a new random variable Z with cumulative distribution function, G given by the product of the cumulative distribution function of each random variable X_i:

$$G(z) = \prod_{i=1}^{n} F_i(z). \tag{2.6}$$

Then, the probability function, g is well determined by the derivative relation with its cumulative distribution function, G:

$$g(z) = \frac{d}{dz}G(z). \tag{2.7}$$

2.4.1 Detection of Logical "0"

A logical "0" is transmitted as silence [64]. This was firstly introduced to save energy and to reduce the interference among different nanodevices. Moreover, it simplifies the symbol detection, enabling non-coherent power detection schemes. When silence is transmitted, the receiver switches on for a time T, where just noise is detected in the receiver. In this case, there is no reason why the components of $\boldsymbol{X}$ might be different. For this we can consider $\boldsymbol{X}$ as a vector with identically N random variables, with probability density function $f_n(y)$.

Particularizing (2.7) for the probability function of $\max \boldsymbol{X}$ in terms of the probability density function $f_n(y)$ of the N identically random variables by:

$$f_{max,n}(y, N) = NF_n(y)^{N-1} f_n(y) \tag{2.8}$$

where N is the number of discrete random variables, $f_n(y)$ refers to the probability density function of a single x_i variable and $F_n(y)$ stands for its cumulative distribution function.

Each X_i corresponds to the square value of the noise signal. This non-white noise is gaussian with a bandwidth provided by the low-pass filter. Gaussian noise is commonly modeled in the literature as a chi-square with $v = 2T_pW$ degrees of freedom random variable [75], with T_p the pulse time and W its bandwidth. This probability density function is expressed in terms of the normalized random variable $Y = 2X/N_{00}$, for a two sided power spectral noise density $N_{00}/2$ and is given by:

$$f_n(y) = \frac{1}{2^{v/2}\Gamma(\frac{v}{2})} y^{(v-2)/2} e^{-y/2}, \quad y \geq 0 \tag{2.9}$$

where Γ is the gamma function, with v degrees of freedom and y the normalized random variable.

In particular, if TS-OOK and ultra-short pulse modulations uses $T_pW = 1$, we can simplify the equation and obtain for $f_{max,n}(y, N)$:

$$f_{max,n}(y, N) = \frac{1}{2} N \Big(1 - e^{-y/2}\Big)^{N-1} e^{-y/2}. \tag{2.10}$$

However, only if the pulse is strictly 100 femtosecond-long, this condition is valid. Since the pulse generated is supposed to be the n-th time derivative of a gaussian pulse. This n-th time derivative is due to the fact that on the one hand, only AC signals can be radiated, and secondly we expect the circuits to be band limited, providing a derivative effect over the signal. Additionally, the second order low-pass filter is just an approximation of an ideal integrator. For this, values of T_pW are expected to be higher. In particular, for a second time derivative gaussian pulse we have $T_pW = 3.5$. For this, there is no closed expression of $f_{max,s}(y, N)$ so the the function must be numerically evaluated.

2.4.2 Detection of Logical "1"

A logical "1" is transmitted by using a femtosecond-long pulse [64]. These pulses are sent spread in time so we reject any interference between consecutive symbols.

The received signal $x(t)$ is noise during most of the time. This is because the time interval, T, is supposed to be around 10 times bigger than the pulse time for future synchronization and implementation purposes. However, during a short time, the signal $x(t)$ turns out to be noise plus signal. This fact lets us to consider two different types of random variables. On the one hand, we model the signal during time where the signal is just noise using N_n independent noise random variables with $f_n(y)$. On the other hand, we model the signal when the pulse is coming using N_s independent random variables with $f_{sn}(y)$ distribution. Since the total number of random variables, N, is proportional to the time interval T, we must always accomplish that $N = N_s + N_n$. Using this model, we can express the random variable defined as the maximum of the received signal $x(t)$ as:

$$\max_N \boldsymbol{X}_{sn} = \max_N \{\boldsymbol{X}_{n,N_n}, \boldsymbol{X}_{s,N_S}\} \tag{2.11}$$

where $\boldsymbol{X}_{sn}$ refers to the vector containing the random variables that model a pulse in reception, $\boldsymbol{X}_{s,N_s}$ stands for the vector of N_s random variables that model $x(t)$ when a pulse is being received. $\boldsymbol{X}_{n,N_n}$ is the vector containing noise with N_n identically distributed independent random variables. The total number of random variables of noise and signal must be kept equal to $N = N_n + N_s$ since N is proportional to the time interval. Then, the probability density function of the random variable $\max x(t)$ can be expressed by:

$$f_{max,sn}(y, N_s, N_n) = F_{max,s}(y, N_s) f_{max,n}(y, N_n) + f_{max,s}(y, N_s) F_{max,n}(y, N_n) \tag{2.12}$$

where $f_{max,sn}$ is the probability density function of the random variable $\max x(t)$ when transmitting a pulse, $f_{max,s}(y)$ stands for the probability density function of the maximum of $\boldsymbol{X}_{s,N_s}$ with N_s random variables, with $F_{max,s}(y)$ its cumulative distribution function, $f_{max,n}(y, N_n)$ the probability density function of $\max \boldsymbol{X}_{n,N_n}$ with N_n random variables and $F_{max,n}(y, N_n)$ its cumulative distribution function. Each component of $\boldsymbol{X}_{s,N_s}$ is characterized by the probability density function $f_s(y)$. Similar to $f_n(y)$, $f_s(y)$ is usually modeled in the literature as a normalized non-central chi-squared distribution with $v = 2T_pW$ degrees of freedom with the normalized random variable $Y = 2X/N_{01}$ for a two sided power spectral noise density $N_{01}/2$ [75]. This is given by:

$$f_s(y) = \frac{1}{2}\left(\frac{y}{\lambda}\right)^{(v-2)/4} e^{-(y+\lambda)/2} I_{(v-2)/2}(\sqrt{(}y\lambda) \tag{2.13}$$

where $\lambda = 2E/N_{01}$ refers to the non-centrality parameter and $I_n(z)$ the stands for the n-th order modified Bessel Function of the first kind. $f_{max,s}(y)$ can be expressed by using (2.8) as:

$$f_{max,s}(y, N_s) = \frac{1}{2} N_s \left(1 - e^{-y/2}\right)^{N_s - 1} e^{-y/2}. \tag{2.14}$$

However, provided that the noise level must be kept lower than the signal level to guarantee a certain SER, $\max_N \boldsymbol{X}_{sn} = \max_N\{\boldsymbol{X}_{n,N_n}, \boldsymbol{X}_s\} \approx \max_{N_s}\{\boldsymbol{X}_s\}$, and then, we can approximate the probability density function by just:

$$f_{max,sn}(y, N_s) \approx f_{max,s}(y, N_s). \tag{2.15}$$

In any case, the signal model, $f_{max,sn}(y, N_s, N_n)$ cannot lead to a closed expression since $F_{sn}(y)$ is not solvable.

2.4.3 Threshold and SER

The performance of the symbol detector can be expressed in terms of the error detection probability of every symbol, and averaging them by their symbol probability. The error detection probability for both symbols is defined as:

$$\begin{aligned} P_{\epsilon|s=0} &= \int_{2V_T/N_{00}}^{\infty} f_{max,n}(y, N)dy \ , \\ P_{\epsilon|s=1} &= \int_{0}^{2V_T/N_{01}} f_{max,sn}(y, N)dy \end{aligned} \tag{2.16}$$

where V_T stands for the threshold, N_{00} and N_{01} refer to the noise level for the symbols "0" and "1" respectively and $f_{max,n}(y, N)$ and $f_{max,sn}(y, N)$ are the probability density functions for the symbols "0" and "1".

The detection threshold is defined as the lowest value that is detected as a pulse. This value is very important in the SER estimation. The SER varies as function of the detection threshold. We define the SER as:

$$SER = P_{\epsilon|s=0}p_{s=0} + P_{\epsilon|s=1}p_{s=1} \tag{2.17}$$

where $P_{\epsilon|s=0}$ and $P_{\epsilon|s=1}$ refers to the detection probabilities in (2.16) and $p_{s=0}$ and $p_{s=1}$ the symbol probability. Optimizing the SER means to optimize the position of the detection threshold. This optimization is not solvable. In the following section, this expression is always numerically evaluated before to provide the optimum performance of the system.

2.5 Performance Evaluation

In this section, we validate the expressions for the probability density functions of both symbols, "0" and "1", throughout simulation. We analyze the performance of the receiver and the symbol detector in terms of SER as function of the channel attenuation and noise.

2.5.1 System Model

To evaluate the model, we have considered the following assumptions in our analysis, numerical evaluation and simulation:

- The path-loss and noise in the Terahertz band are computed by using the models introduced in [4]. A standard medium with 10% of water vapor is considered. These parameters are expressed in terms of the distance. Different distances provide different channels in terms of path-loss and noise.
- Although the channel is asymmetric [4], we suppose, in case it is not explicitly commented, the worst case scenario where the noise level for both symbols is considered the same,and we refer this noise level as $N_0 = N_{00} = N_{01}$. This is since a pulse from another nanodevice can excite the channel just before the symbol "0" is transmitted. However, interference between nanodevices has not been considered because TS-OOK provides an almost orthogonal channel [64], and then, collisions between pulses are very unlikely.
- No internal noise inside the nanodevice is consider, but only the channel noise has been modeled in the numerical and simulation results, since no specific technology has been considered and to the best of our knowledge, there is no a noise characterization for graphene technology.
- The transmitter encodes logical "1" by using 1 pJ 100 femtosecond-long gaussian pulses. The second time-derivative of the gaussian pulse is supposed to be detected in the receiver. The logical "0" is transmitted as silence.
- The receiver is perfectly synchronized with the transmitter, the time interval is always centered in the pulse.
- The symbol probabilities are considered equal for the logical "1"s and "0"s. $p_{s=0} = p_{s=1} = 0.5$.

2.5.2 Model Validation

A simulation of the channel an receiver has been done to validate the expressions provided in Sec.2.4 for the symbols "0" and "1". In this simulation, the second time-derivative of a 100 femtosecond-long gaussian pulse has been implemented. The values of the energy per bit and the noise level chosen belong to a distance between devices of 66 mm. This distance, as shown in the following evaluations, provides a $SER = 2 \cdot 10^{-4}$. Using this pulse, the product pulse time - bandwidth is $T_pW = 3.5$. The normalized results of the simulations are shown overlapped over the numerical results in Fig. 2.5. The simulation results provide the random

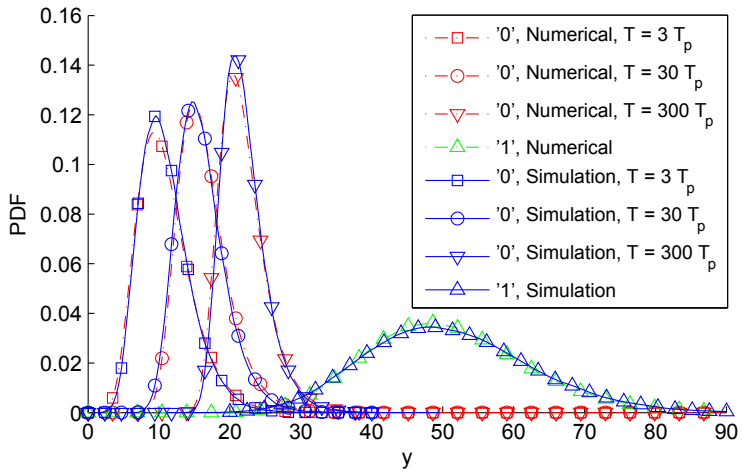

Figure 2.5: Probability density function of $\max x(t)$ when receiving logical "0"s and "1"s for a distance of 66 mm

variable $\max x(t)$. To match results, we have appropriate normalized this output variable to $Y = 2X/N_{00}$ when a logical "0" is received or to $Y = 2X/N_{01}$ when the pulse received is a logical "1".

Logical "0"

As shown in Fig. 2.5, the logical "0" is represented for three different time intervals $T = \{3, 30, 300\}\ T_p$. These three time intervals need for the analytical model $N = \{2, 15, 110\}$, which validates the fact that N is proportional to T. As shown, the average value presents logarithmic growth with this time interval.

Logical "1"

The logical "1" needs $N_s = 2$. It does not present any variation with the time interval. This validates the approximation in (2.15). To observe the effect of the time interval in the variation of the logical "1" requires very large time intervals or very low E/N_0 ratio, which leads to very bad values of SER. This last particular case is out of our study because a SER of around 10^{-3} to 10^{-4} is the usual target in communications. In particular, the signal to noise ratio used to estimate these number gives a $SER = 2 \cdot 10^{-4}$.

2.5.3 SER Estimation

Fig. 2.4 shows the SER estimation as function of the distance. In the figure, three curves, referred as *Max*, show the proposed architecture estimated SER for the values of $n = T/T_p = \{3, 30, 300\}$. Equivalently, three curves for the same values of n are shown for classic receiver architectures based on integration over the time interval T, referred as *Int*. As the figure

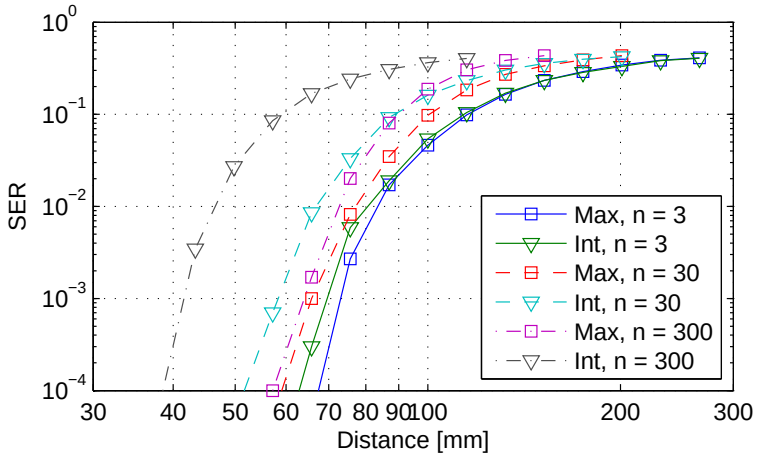

Figure 2.6: Comparison between the SER provided by the proposed receiver and current receiver for different time intervals

shows, the proposed receiver outperforms the existing receivers increasing in up to 50% the maximum distance when $n = 300$, to guarantee a SER of $SER = 10^{-4}$.

Moreover, from the figure, we observe the strong impact that the molecular absorption has over the attenuation and noise in terms of the distance. A distance increase of around a 10% drops the SER in several orders of magnitude.

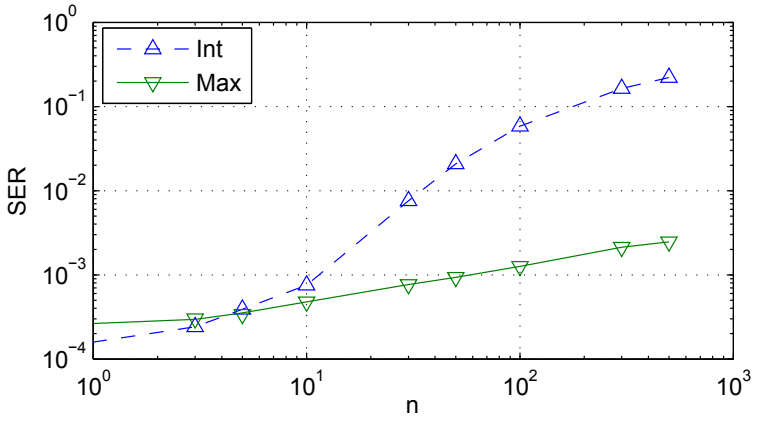

Figure 2.7: Comparison between the SER provided by the proposed receiver and current receiver in terms of $n = T/T_p$

Alternatively, we also show the dependence of the SER with the with the ratio n. This dependence is shown in Fig. 2.7 for a fixed distance of 66 mm. As shown, when the time interval, T is similar to T_p, we obtain similar performance with both receivers. However as the ratio between times, n, increases the proposed receiver outperforms the previous architecture. For nanodevices, where simplicity and consumption must be kept as the main constraints, increasing the time interval means significantly relax the design conditions.

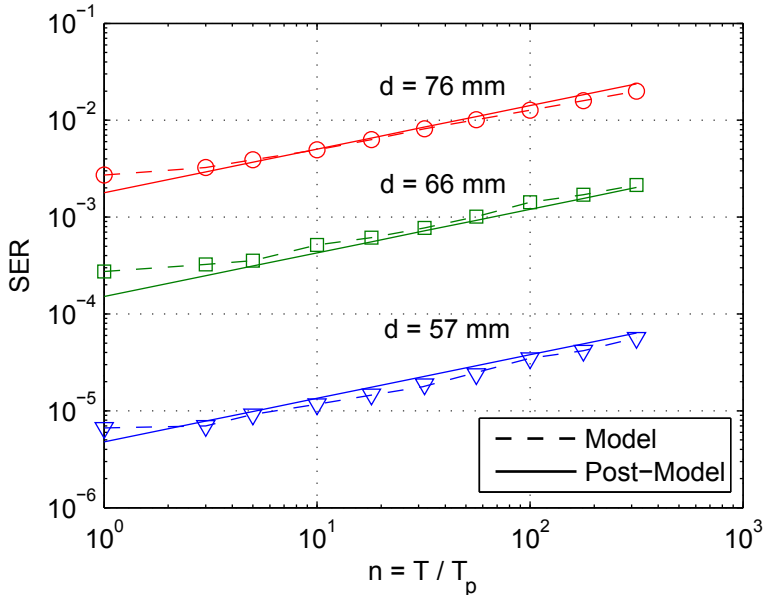

Figure 2.8: Comparison of the model and post-model results for different distances between devices.

2.5.4 SER Post-simulation Model

The expressions for the probability density function of the functions $\max \boldsymbol{X}|s = 0$ and $\max \boldsymbol{X}|s = 1$ are composed by the maximum of a large number of chi-square distributions. This fact makes the SER estimation difficult to calculate. For this purpose, we propose to model the SER *a posteriori*, based on the observed dependency with n.

Fig. 2.7 shows that there is a log-log behavior in the SER versus the ratio $n = T/T_p$. Moreover, this log-log behavior is approximately constant for any ratio E/N_0, and even for different noises for "1"s and "0"s, N_{01} and N_{00}. This log-log relation provides a relation between the SER at two different ratios n_1 and n_2 given by:

$$SER_{n_2} = r^{0.45} SER_{n_1} \tag{2.18}$$

where $r = T_2/T_1 = n_2/n_1$ is the relation between time intervals.

Then, computing the Engler model [76] to calculate the SER for $n = 1$ with parameter $TW = 3.5$. And then using (2.18) we can obtain the SER for any distance and ratio n. Fig. 2.8 shows a comparison between the original model and its post-simulation model. As shown, the post-simulation model matches with the expected value for any of the three distances.

2.5.5 Maximum Bitrate

The TS-OOK modulation spreads femtosecond-long pulses in time. This time-spread is characterized by a parameter $\beta = T_s/T_p$ and it is usually in the order of $\beta \sim 1000$. For this, in the previous sections, different symbols are considered independent. Although this architecture

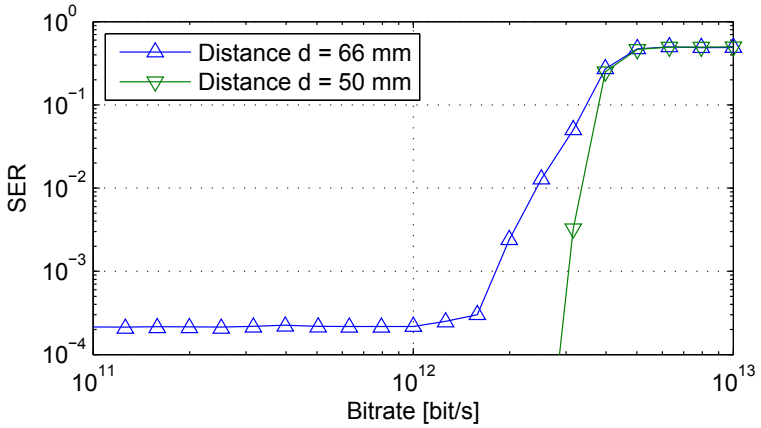

Figure 2.9: SER in terms of bitrate

is proposed mainly to support TS-OOK, this transceiver can also support bitrates up to few Terabits per second. When the bitrate increases and it gets close to $\beta \sim 1$, the non-idealities of using a low-pass filter to replace an ideal integrator plus the overlapping of different pulses affect the system providing an inter symbol interference (ISI). For this, we have performed a simulation of the Terahertz channel and the receiver architecture considering the overlapping effects between symbols. Fig. 2.9 shows the achievable SER in terms of bitrate for two different distances between nanodevices. As shown, until approximately $R = 2$ Tbit/s the SER is mainly limited by noise, so the SER is kept constant at $SER \approx 2 \cdot 10^{-4}$ for a distance $d = 66$ mm. Then, as soon as the bitrate increases, the receiver is highly affected by the ISI, dropping the SER to $SER = 0.5$ when $R = 5$ Tbit/s. Concerning the distance $d = 50$ mm, the ratio E/N_0 is high enough to neglect the SER when the system is limited by noise. However, as shown in the figure, when the ISI is affecting the receiver, the SER tends to the same values, presenting a $SER = 0.5$ when $R = 5$ Tbit/s.

2.6 Conclusion

In this chapter, we propose a novel transceiver architecture for electromagnetic nanonetworks in the Terahertz channel. This architecture simplifies the basic structure of the transceiver, tailoring the easy integration of impulse-based modulations, such as the recently introduced TS-OOK modulation for nanodevices. Our solution decouples the integration, threshold comparison and the sampling time and outperforms previous receivers proposed in other impulse-based communications communications schemes applied in the Terahertz band.

We first describe each block of that defines the transmitter and receiver architectures. We mathematically describe the symbol detection, as well as, we analyze the probability density functions of the received symbols and validate this results through simulation. Since the different distances between nanodevices define different channels in terms of path-loss and noise, we provide the symbol error rate estimation in the Terahertz band as function of the

distance between nanodevices. Moreover, we provide a post-simulation model to simplify the estimation of the symbol error rate over the Terahertz channel. Finally, although, this simple transceiver is conceived to support time-spread modulation schemes, we explore the possibilities of this transceiver architecture when the bitrate is increased up to tens of terabits per second, showing that the effects of the inter symbol interference limits the performance at these bitrates.

The results show that, in the Terahertz channel, the novel transceiver architecture for nanodevices outperforms existing impulse-radio based transceiver architectures reducing the symbol error rate and increasing the transmission distance. Moreover, we show that the proposed nano-transceiver can also support bitrates of up to tens of terabits per second for distances in the order of tens of millimeters using very simple modulation schemes.

Chapter 3

A Novel Symbol Time Synchronization Scheme for Electromagnetic Nanonetworks in the Terahertz Band

3.1 Introduction

As seen in the previous chapters, the Terahertz band provides a huge bandwidth that can be used in the short range either to support very high transmission rates or to simplify the communication paradigm between two nanodevices using simple modulation schemes. In Chapter 2, we proposed a novel transceiver architecture that is supposed to support pulse-based modulation schemes. As an example, the transceiver architecture has been evaluated under the conditions and particular properties of TS-OOK.

In the previous chapter, the analysis of the receiver architecture and the symbol detection scheme has been performed assuming that the receiver is perfectly synchronized to the transmitter and the upcoming pulse is supposed to arrive right in the middle of the observation time interval.

A seen in Chapter 2, in order to save energy, the transceiver disables the receiver when no symbol is supposed to arrive, an it switches it back on to receive the next symbol. Although we have commented that the All-Digital architectures avoid the use of high frequency sources to feed the antenna, the nanodevice must have an internal one to compute and manage the transmission. However, this second high frequency source is not subject to the same constraints since the power needed to feed the nano-antenna is bigger than the power needed to enable the digital circuitry.

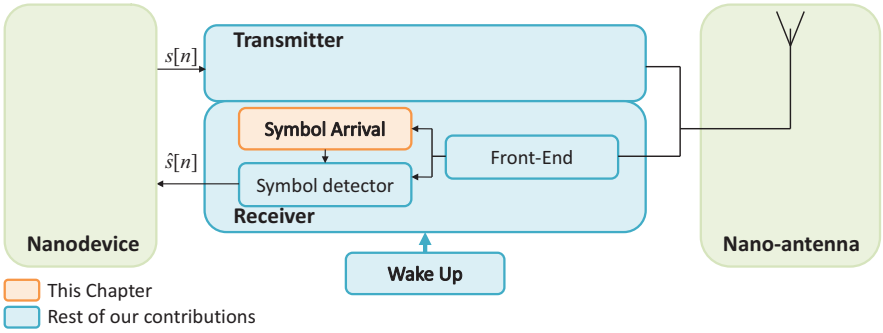

Figure 3.1: Context of the work presented in this chapter. The symbol time synchronization block in the transceiver and nanodevice architecture.

As seen in Sec. 1.2.1, there are currently several promising options for the future implementation of Terahertz sources in the nanoscale. Some of the more promising are the RF NEMS technology, where the authors in [52] reach the conclusion that with Graphene RF-NEMS, oscillation at frequencies beyond 1 Terahertz are possible, this alternative is very promising because it will enable full graphene systems. Alternatively, the STNO technology also provides a framework for Terahertz oscillations. In particular, authors in [54, 56] expect the STNOs to operate at Terahertz frequencies as well.

In any case, both technologies are sensitive to changes in their environment. Energy fluctuations and physical or mechanical efforts over the oscillator can modify the oscillation frequency or phase in the nanodevice. As seen in 1.2.4, the maximum energy that a nanodevice can store is comparable to a the energy needed to send just a few number of packets. This energy limitation implies frequency drifts that both nanodevices, emitter and receiver, must be able to cope with to guarantee the successfully transmission of the information.

The energy drifts imply that when a transmission is started, both transmitter and receiver must synchronize their frequencies before sending the information. In current pulse-based communication schemes, the frequency synchronization is avoided by implementing transceiver architectures with crystal oscillators [69], so the receiver reduces the necessity of implementing any PLL circuit that reduces performance, needs some time to synchronize. Additionally it PLL synchronization is not recommended in carrierless communications. However, the absence of nano-crystal oscillators and the frequency drifts of the promising nanoscale technologies, disables this implementation.

Moreover, not only the frequency must be estimated, but also de time of arrival. In fact, using TS-OOK as an example of impulse-based modulation scheme for EM nanonetworks, the pulse time is set to around one thousandth of the symbol time. This is, the transmitter is in silence and it only transmits power for a very short time. As seen in Chapter 2, the shorter the time interval where the receiver expects the pulse, the better SER will obtain. However, since the modulation is On-Off instead of a pulse position scheme, we can estimate the frequency and the pulse position at the same time.

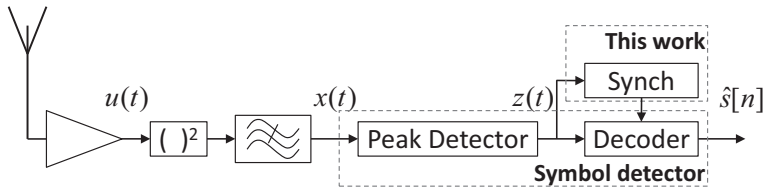

Figure 3.2: Receiver Block diagram Architecture

In this context, we propose a novel frequency estimation scheme for nanonetworks designed to activate and deactivate the receiver accordingly to provide its best performance over the TS-OOK modulation scheme introduced in [4]. In fig. 3.1 we locate this block and its main contributions in the nanodevice architecture.

Our main contributions presented in this chapter can be summarized as follows:

- We develop an algorithm for the frequency estimation using a very short preamble of pulses and an algorithm to adaptively follow the clock drifs.
- We analytically analyze the impact of these algorithms over the Packet Error Rate (PER) and validate these results with simulations.
- We compare the performance of the transceiver architecture with and without this symbol time synchronization scheme.

The rest of this chapter is organized as follows. In Sec. 3.2, we describe the receiver architecture where the synchronization scheme is built on top. The two stages of the synchronization are proposed in Sec. 3.3 and Sec. 3.4. In Sec. 3.5, we validate the algorithms and evaluate the performance of this synchronization scheme. We conclude the chapter in Sec. 3.6.

3.2 Receiver Architecture

We build this frequency estimation on top of the receiver architecture proposed in Chapter 2. However, we focus on specific properties that this architecture can provide. This architecture, shown in Fig. 3.2, has been especially proposed to provide simplicity and ease of integration, robustness in the reception, novel synchronization capabilities and specifically proposed to handle TS-OOK modulated signals. This receiver consists of:

- Terahertz Front-End: Input filter and amplifier to match the antenna impedance and to condition the input filter
- Power Detector: Non-coherent detection based on power detection.
- Low-Pass Filter: Proposed as an approximation of a continuous-time integrator.

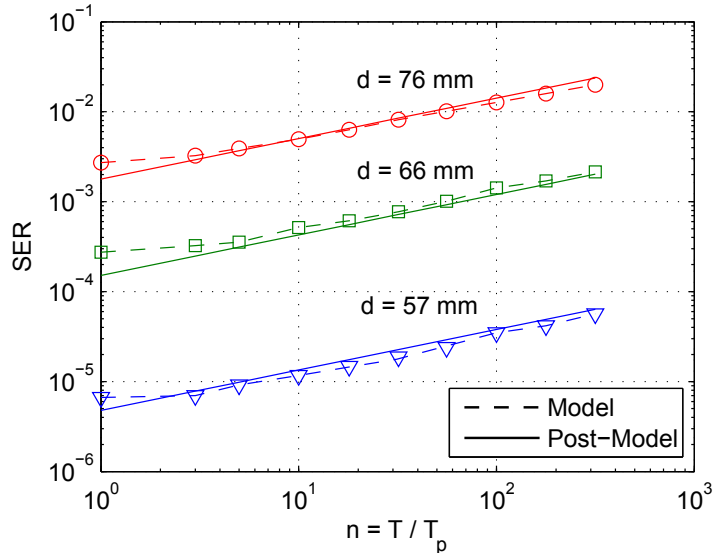

Figure 3.3: Comparison of the model and post-model results for different distances between devices.

- Peak Detector: This block fixes its output, $z(t)$ to "1" until an external block resets it when its input signal, $x(t)$, is above a threshold. Otherwise is kept as "0". This comparison is continuous in time.
- Synch: Provides the frequency estimation. This block switches on and off the receiver. This block is the main aim of this chapter.
- Decoder: Here the signal $z(t)$ is decoded into $\hat{s}[n]$ by providing the logic values "0" and "1" when the synchronization block decides that a new pulse has arrived.

3.2.1 Symbol Detector

The symbol detector used in this receiver architecture consists of the peak detector, the decision made in the decoder and the sampling provided by the synchronization block. If at any instant of time, the input at the peak detector is above a prefixed threshold, its output is fixed to 1 until an external circuit resets it, otherwise is kept as zero.

In Sec. 2.5, we determined that increasing the time interval T of observation implied a worsening in terms of SER.As shown in Fig. 3.3, We approximated the SER for a time interval T_2 by the relation between time intervals r as:

$$SER_{T_2} \approx r^{0.45} SER_{T_1} \tag{3.1}$$

where T_1 is the previous time interval, and r is defined as $r = T_2/T_1$. The SER approximated by this equation is the result of the optimum SER for a specific time interval T_2 in case the probability of receiving a logical "0" is equal to the probability of receiving a "1".

In the following sections, we explore the implication of varying the time interval to adaptive match the frequency during the packet reception. However, we assume that optimize the

receiver each time the time interval is modified is not feasible. Thus, the aim of this chapter is to find for which time interval the receiver must be optimized in order to provide the system the best performance, although the time interval is variable.

To do this, we assume that any time interval is based on a integer number of sub-time intervals T_I. This sub-time interval is fixed by the operating frequency of the nanodevice. Then, in general, a time interval T can be expressed as $T = KT_I$.

The error probabilities of detecting a logical "0" or a logical "1" can be expressed by the error probability of detecting these logical values in each sub-time interval. In general, an interval T is composed by K sub-time intervals. In case of the logical "0", every sub-time interval must be silence, while in the case of the logical "1", one of the sub-time interval carries the femtosecond-long pulse, while the other sub-time intervals are modeled as silence. Thus, the error probabilities in terms of the error probabilities of the sub-time intervals are given by:

$$\begin{aligned} P_{\epsilon|s=0} &= 1 - (1 - p_0)^K \approx Kp_0 \\ P_{\epsilon|s=1} &= p_1(1 - p_0)^{K-1} \approx p_1 \end{aligned} \tag{3.2}$$

where $P_{\epsilon|s=0}$ and $P_{\epsilon|s=1}$ are the error probabilities of detecting a "0" and "1" respectively in the time interval and p_0 and p_1 stands for the error probability of detecting a "0" and "1" respectively in one of the K time sub-time intervals.

Probabilities p_0 and p_1 are kept constant throughout the reception. These probabilities are optimized so that for an optimum K_{opt}, probabilities $P_{\epsilon|s=0}$ and $P_{\epsilon|s=1}$ are equal. Then, for time intervals shorter than this optimum, $K < K_{opt}$, the error probability of the logical "1" is bigger than the "0", whereas when the time interval is larger than the optimum, $K > K_{opt}$, the error probability of the logical "0" is bigger.

3.3 Frequency Estimation

Nanodevices are expected to be densely deployed to cover large areas [1]. The time spreading of the TS-OOK modulation scheme provides almost orthogonal channels for this neighboring nodes in the nanonetwork. This is that although some nanodevices are transmitting at same time, it is very probable that the reception can be successfully received. This almost orthogonality comes from the time spreading. To satisfy the time multiplexing in TS-OOK, the time interval, T, where a pulse must arrive, defined in the previous chapter, must accomplish $T \ll T_s$. To satisfy this condition, the receiver has to sample its input at a sampling frequency $f_0 = 1/T$.

The limitations in size, cost, energy and the use energy-dependent oscillators, such as RF NEMSs and STNOs lets us assume that different devices operate at different, but close, fre-

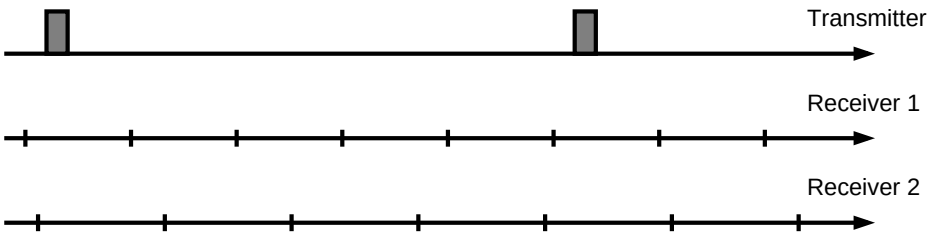

Figure 3.4: Example of the relative frequencies. The transmitter sends pulses each 5 sampling periods of receiver 1 and 4 sampling periods of receiver 2.

quencies. Additionally, any solution must be kept as simple as possible, since simple structures are more likely to succeed in the future design of nanodevices.

This difference between operating frequencies makes the transmitter and receiver nanodevices to synchronize their frequency before the packet transmission starts. Additionally, because of the time spreading properties, the receiver has to estimate also the time of arrival of this pulse. In other words, the receiver not only must synchronize in frequency but also in phase. We also assume that a nanodevice cannot keep the synchronization for different transmissions, so every packet transmission will include a symbol time synchronization preamble.

3.3.1 Relative Frequencies

TS-OOK defines the parameter β as $\beta = T_s/T_p \approx 1000$. Assuming that the receiver architecture uses a time interval defined as $T = nT_p$, the receiver counts approximately β/n periods between pulses.

As an example, in case the time interval is equal to $T = 10T_p$, there are 100 time periods between consecutive symbols. To switch On and Off the receiver in order to correctly receive the upcoming pulses, the receiver has to count up to 100, switch On, check if there is a new pulse and switch back Off. In this example, the different frequencies between nanodevices makes that instead of exactly 100 pulses, the receiver can estimates a slightly different period, such as 95 or 105, also due to possible drifts, this value may change during the reception.

In the following, we refer the number of slots estimated by the receiver j between consecutive pulses as $\hat{N}_j$, which we assume to be modeled as a random variable with gaussian distribution. To show the effect of different frequencies, Fig. 3.4 shows an example where a transmitter is sending pulses, and two receivers are listening at the channel. Even though the receivers are operating at different frequencies (time slots), each receiver can estimate the incoming rate as function of their own frequency. The receiver 1 detects a bitrate of $\hat{N}_1 = 5$, whereas the receiver 2 detects a bitrate $\hat{N}_2 = 4$. Thus, a third pulse is expected to arrive after $N = 5$ or $N = 4$ time slots, for the receiver 1 and 2 respectively.

This counting is referred as relative frequencies. In this case, nanodevices do not know the frequency at which the other nanodevices are operating. Instead, when a nanodevice

must send information it just sends it using its specific frequency (in the example above, the nanodevice would send a symbol every 100 time periods) while the target nanodevice which is listening to the channel it estimates the incoming frequency in terms of number of time periods (in the example above, this nanodevice would listen to the channel every 95 time periods).

Counting time periods for the estimation of the relative frequency carries an inherent estimation error since the counting between consecutive pulses is an integer number. This means that the number of sampling periods, or relative bitrate, $\hat{N}_i$, that counts the receiver i, can be expressed as:

$$\hat{N}_i = \frac{N_j T_j^s}{T_i^s} + \epsilon \tag{3.3}$$

where T_j and T_i are the sample period of the transmitter j and the receiver i, respectively, N_j refers to the relative bitrate of the transmitter j and $\epsilon \in (-1, 1)$ refers to the error in the estimation and makes $\hat{N}_i \in \mathbb{Z}$.

We assume that the relation between time symbols is characterized by a random Gaussian variable while the error ϵ provided by this estimation is uniformly distributed in one count. To reduce this error, we can oversample at a higher frequency so this ϵ in terms of time is reduced. This oversampling can be interpreted in two different ways: on the one hand, oversampling means to just look at every time period more than one time, which is feasible with the receiver architecture proposed to support this symbol time synchronization. On the other hand, we can also reduce of the time interval T. Notice that, in both cases, the sampling period is limited by the pulse time. However, increasing the sampling frequency is not always achievable or practical.

In this chapter, we suppose that the time interval T is fixed and any possible frequency drift can just affect the counting in just one period time for consecutive symbol periods. On the contrary, this time can always be increased to satisfy this condition.

3.3.2 Symbol Time Estimation Algorithm

To reduce the error in the estimation, we propose the use of an ML estimator. In particular, when For this, an ML estimation, over a synchronization preamble is proposed to reduce the error in the estimation. The ML estimation is defined as follows:

Supposing that there is a sample $x_1, x_2, ..., x_n$ of observations, coming from a distribution of known family $\{f(\cdot|\theta), \theta \in \Theta\}$, but unknown the exact probability density function f_0. The value θ_0 is the unknown value that must be estimated. We need to find some estimator $\hat{\theta}$ which would be as close as possible to θ_0.

We define the *likelihood* function as:

$$\mathcal{L}(\theta|x_1, x_2, ..., x_n) = \prod_{i=1}^{n} f(x_i|\theta) \tag{3.4}$$

The method of maximum likelihood estimates θ_0 by finding the $\hat{\theta}$ that maximizes the likelihood function, $\mathcal{L}$:

$$\hat{\theta}_{mle} = \arg\max \mathcal{L}(\theta|x_1, x_2, ..., x_n) \tag{3.5}$$

Since the parameter to estimate is the number of time periods which is modeled as a gaussian variable of $\mathcal{N}(N, \sigma)$, considering that we have $N_1, N_2, ..., N_n$ individual time estimations, we obtain:

$$\hat{N} = \sum_{i=1}^{n} N_i/n. \tag{3.6}$$

To obtain this estimation of the symbol time period, a synchronization preamble is sent before the transmission. The fact that logic "0"s are transmitted as silence and logic "1"s as pulses, makes the logic "1"s to help in the receiver to synchronize whereas the logic "0" provides uncertainty in the next symbol. For this reason, the synchronization preamble must contain N_{synch} number of ones, "11...1". Using this preamble, we can reduce of the error ϵ in according to:

$$|\epsilon| < \frac{1}{N_{synch} - 1}. \tag{3.7}$$

This is assuming an error-free situation. In the real case, the error can be out of this interval. In the following sections this probability is referred as p_{synch} which models the probability of estimating the frequency with an error ϵ.

The receiver cannot be listening the channel during all the time between symbols because this supposes extra power consumption, it increases the error probability and disables the time-multiplexing properties in the channel.

The receiver must be kept in standby until the new pulse is about to arrive. Then, when the receiver expects to receive the next pulse, it switches on and listens for a time long enough to make sure the pulse is going to arrive. To determine the length of this time interval we suppose an initial error between frequencies. This error is considered as an external parameter provided by the accuracy and future fabrication processes used to implement the nano-oscillators. However, in general, we consider that this error is characterized by a centered gaussian random variable with standard deviation σ, $\mathcal{N}(0, \sigma^2)$.

Then the number K of subintervals is fixed to:

$$K = \lceil N_s + n\sigma + 1/2 \rceil - \lfloor N_s - n\sigma - 1/2 \rfloor \tag{3.8}$$

where N_s is the internal time slot, n refers to the confidence interval and σ stands for the standard deviation in between frequencies. $\lceil\ \rceil$ and $\lfloor\ \rfloor$ are the ceiling and floor functions respectively. The value of n must be chosen according to the desired performance. Small

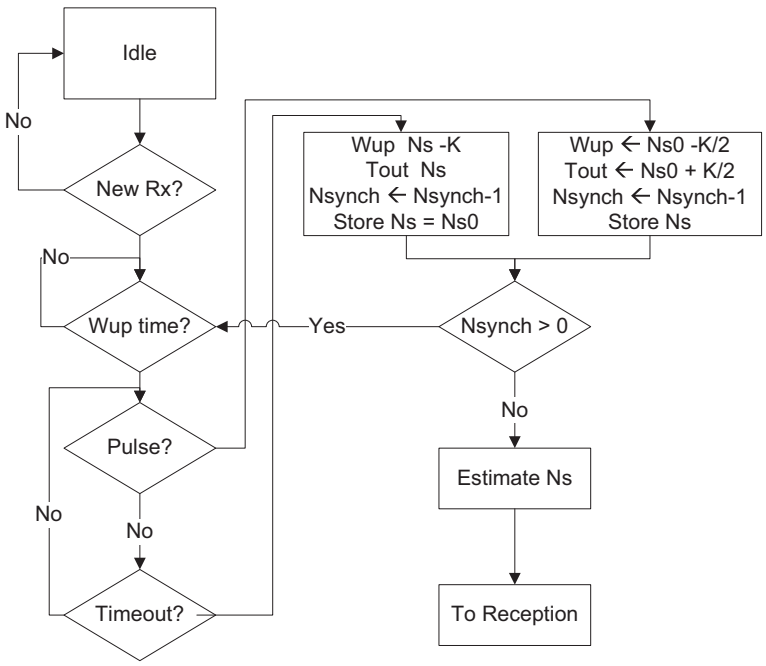

Figure 3.5: Proposed algorithm to accordingly switch On and Off the transceiver while the receiver is estimating the frequency.

values of n will limit the synchronization probability while large values of n, which make K very large, increases the chances of being affected by noise or interferences.

The algorithm to switch On and Off the transceiver during the frequency estimation preamble is described in Fig. 3.5. As shown, during this frequency synchronization preamble, the number of time periods between pulses is fixed to N_{s0}. This number is actually the nominal counting of the receiver nanodevice. Then, the algorithm wakes-up the receiver from the Idle state in case a pulse is about to come. In fact, the receiver will wake up $K/2$ time periods before the expected time of arrival. If after K time periods, no pulse has been received, the receiver assumes the center of the time interval as the actual arrival. Then, the receiver sets the wake-up for the next pulse arrival N_{s0} time periods after the arrival of this pulse, with a time interval K.

3.4 Adaptive Frequency Correction

The receiver must be able to follow the frequency drifts and the frequency estimation error in order to successfully decode the message. In this case, we make use of the particular properties of the receiver architecture introduced in Chapter 2. This receiver is able to detect the arrival of only the first pulse during a time interval, with a time resolution T_I. In case that because of noise or interferences, multiple pulses arrive at the receiver, only the first pulse is detected. However, this detection does not suffer of dead zones where the pulse can not be properly

detected between time intervals. So consecutive sub-intervals can be evaluated with a single receiver.

The sub-interval T_I is characterized by a p_0 and p_1, which is fixed during all the reception. We must estimate a time interval wide enough to ensure the pulse arrives inside the interval. This time interval is composed by an integer number K_i of time sub-intervals. Then, we sample the output every T_I until a pulse has arrived or until we reach the end last sub-interval. If a pulse has arrived, we decode the symbol as "1" and we center the next time interval after N_s time periods after the arrival with K_{i+1} interval width. Otherwise, the symbol is decoded as "0" and the center of the next time interval is set $N_s T_I$ after the center of the current interval.

When the channel is subjected to noise or interferences, if K_i is large, the probability of detecting a pulse is increases. Since the expected time of arrival of the next pulse depends on the previous detection, the detector can start following noise level. For this, the size K_i must be kept as small as possible to avoid errors that can desynchronize the reception. However, while the logic "1"s helps the receiver to synchronize, the logic "0" provides uncertainty in the next symbol. To keep the K_i as small as possible but able to follow the frequency drifts even if the symbols are "0", we propose an adaptive algorithm.

3.4.1 Adaptive Correction Algorithm

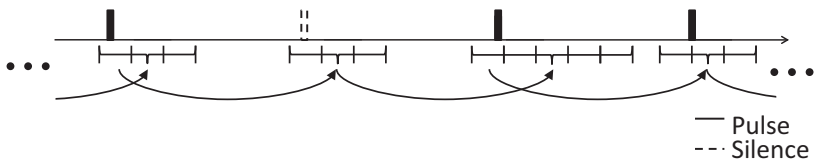

Figure 3.6: Example of the of the algorithm. "1"s reduce uncertainty, "0"s produce it.

Since only "1"s can help in resynchronize the receiver, the more consecutive "0"s received, the more uncertainty we have in the next symbol time of arrival. To estimate the expected time of arrival of the next pulse, the adaptive estimation must keep track of the number of consecutive "0"s that the receiver has decoded. This is referred as n_{zeros}. Thus, supposing the symbol i, the time interval for the following symbol is $K_{i+1}T$, where K_{i+1} is given by:

$$K_{i+1} = \lceil (n_{zeros}+1)(\hat{N}_s + \epsilon) + 1/2 \rceil - \lfloor (n_{zeros}+1)(\hat{N}_s - \epsilon) - 1/2 \rfloor \tag{3.9}$$

where $\lceil\ \rceil$ and $\lfloor\ \rfloor$ denote the ceiling and floor functions respectively, $\hat{N}_s$ is the inverse of the estimated relative bitrate, $\hat{\epsilon}$ stands for the error associated in the estimation of $\hat{N}_j^s$, which is provided by the synchronization preamble, and n_{zeros} refers to the number of consecutive zeros received. Moreover, each time a logic "1" is received, the error associated to the time resolution is represented by the addition of $1/2$ to each side of the interval.

In both cases, $\hat{N}_s$ is needed since not only the width of the error is needed, but also the position. As an example of this adaptive estimator, Fig. 3.6 shows for $\hat{N}_s \in \mathbb{Z}$ and $\hat{\epsilon} = 1$

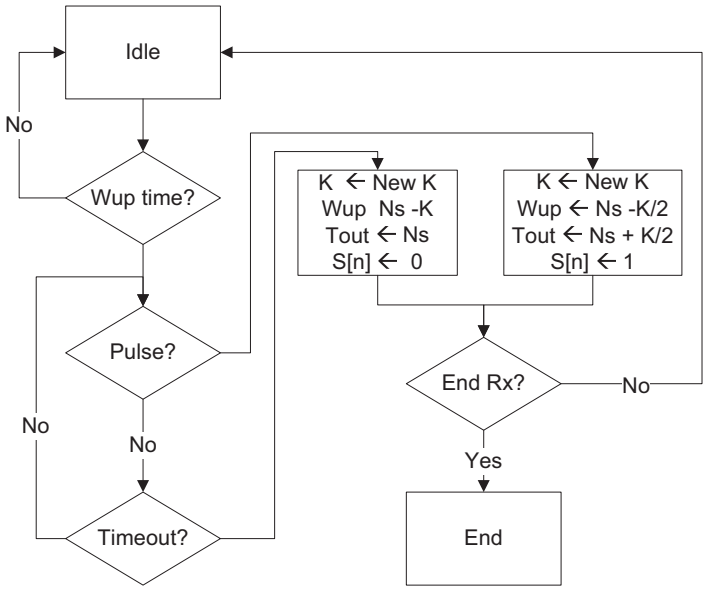

Figure 3.7: Proposed algorithm to handle the available frequency drifts and estimation errors while the reception of a new packet.

how the adaptive estimator evolves of the interval in the reception of the sequence "1011". In the figure, the curved line represents the time $T_s = N_s T_I$, which is much larger than the time interval. Additionally, Fig. 3.7 shows the algorithm proposed to follow the drifts and estimation errors.

To optimize the SER for a given distance, we need to estimate the average number of sub-intervals K. This average number of sub-intervals, referred as $\overline{K}$, is a key parameter to unbalance the error probabilities p_0 and p_1 and, then, to optimize the synchronization scheme. $\overline{K}$ is given by:

$$\overline{K} = \sum_{n=0}^{\infty} p_n E[k_n] = 2\left(1 + \frac{\hat{\epsilon}}{P_{s=1}}\right) \tag{3.10}$$

where $P_{s=1}$ stands for the symbol "1" probability, $E[k_n]$ refers to the average value of K_i with n consecutive zeros received before the current symbol and p_n is the probability of receiving n_{zeros} consecutive zeros which is given by:

$$p_n = P_{s=1} P_{s=0}^n. \tag{3.11}$$

Since the receiver just detects the first pulse received during a time $K_i T_I$, the time that the pulse has arrived determines the estimation of the next pulse. Notice that if an error during the reception of a "1" in a sub-interval of silence, the symbol can be decoded correctly, but the error can desynchronize the receiver. In other words, these errors affect in the error of the consequent symbols. For this, instead of optimizing the SER for the time interval $\overline{K} T_I$,

we must optimize it to have for a time interval $\overline{K}$, the same error probability for the logical "0" than for the zeros. This is described by:

$$p_0 \frac{2\overline{K}-1}{2\overline{K}} = p_1 \frac{1}{2\overline{K}}. \tag{3.12}$$

where the error probabilities p_0 and p_1 are balanced for that function. This is since in an interval $\overline{K}T_I$, $\overline{K}$ "0"s are detected if the symbol was "0", while one "1" and $\overline{K}-1$ "0"s if the symbol was "1". This consideration makes to eventually optimize the SER for a $r = 2\overline{K}-1$, where r stands for the relation $r = T2/T_I$.

3.4.2 Packet Error Rate Estimation

The estimated packet error rate using this adaptive frequency correction, can be expressed by the p_0 and p_1 from (3.1) and (3.2) for a $r = 2\overline{K}-1$. Then, estimating the SER for a time interval K again in (3.2). Eventually, and considering the synchronization probability, we can evaluate the Packet Error Rate (PER) by:

$$PER = 1 - p_{synch}(1 - SER)^{N_{bits}} \tag{3.13}$$

where N_{bits} is the number of bits that a packet has without considering the synchronization preamble.

Since the time interval KT_I is variable, the symbol error rate varies along the reception. However, as it is shown in he following sections, the estimation of the PER by the average time interval $\overline{K}T_I$ provides a very good approximation.

3.5 Performance Evaluation

3.5.1 System Model

- The path-loss and noise in the Terahertz band are computed by using the models introduced in [4]. A standard medium with 10% of water vapor is considered.
- The transmitter encodes logical "1" by using 1 pJ 100 femtosecond-long gaussian pulses. The second time-derivative of the gaussian pulse is supposed to be detected in the receiver. The logical "0" is transmitted as silence. The symbol probabilities are considered equal for the logical "1"s and "0"s. $p_{s=0} = p_{s=1} = 0.5$.
- The SER estimation is performed by using the receiver architecture from Chapter 2.
- If the SER is not specified, we consider $SER_{T_I} = 10^{-4}$.
- No correction algorithms are considered. Thus, a single error in the transmission of a packet makes the packet to be unsuccessfully decoded.

3.5.2 Frequency Estimation

The algorithm proposed for the frequency estimation in Sec. 3.3 keeps the number of intervals fixed while the frequency is being estimated and adjusted. This fact implies that the performance in the synchronization probability depends on the maximum acceptable initial drift between the incoming and the internal frequencies. In this evaluation, the frequency drift between emitter and transmitter is supposed to have a normal distribution in terms of number of sub-intervals, $\mathcal{N}(0, \sigma^2)$. The width of the time interval is chosen to satisfy, at least, a synchronization error probability of $p_{no\ synch} = 10^{-3}$ in error-free situation.

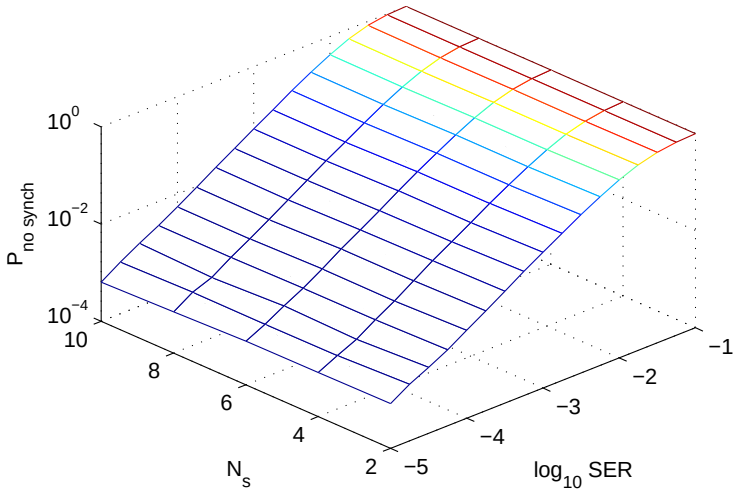

Figure 3.8: Probability of no synchronization as function of the SER in the channel for different lengths of the synchronization preamble.

Fig. 3.8 shows the synchronization error probability as function of the channel degradation in terms of SER for different values of the synchronization preamble length. To compute this probability, we have supposed that the frequency drift is characterized by the following $\sigma = 10$. This synchronization probability refers to the probability that the receiver cannot correctly estimate the symbol rate with a maximum error of ϵ. As shown, although, short preambles should present worse synchronization ratios, this probability presents a quasi-independent relation with the number of symbols for synchronization N_{synch}. The reason is that the growth of ϵ is taken into consideration, so for low values of N_{synch} the maximum acceptable error is larger. Moreover, as sh as the SER is already unbalanced, as shown in 3.4, reducing p_0 in the case of large ϵ.

3.5.3 Adaptive Frequency Correction

The adaptive frequency correction has been evaluated as the optimal packet error rate (PER) achievable. This PER evaluation is shown in Fig. 3.9 for a fixed distance between nanodevices of $d = 60$ mm, with $T_I/T_p = 20$, an error $\hat{\epsilon}$ provided by the Frequency estimation and the

asymmetric K parameter. As seen, there is a minimum in the PER for a given K. This is since the channel is usually in silence, so unbalancing the probabilities reducing the error probability p_0 improves the global PER. However, unbalancing the probabilities has a negative effect in the global SER, so that the PER presents this optimum value.

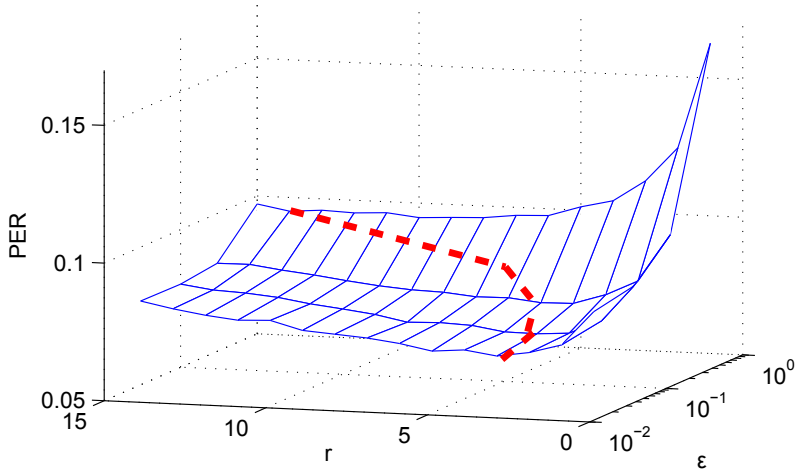

Figure 3.9: PER as function of ϵ and the parameter r used to unbalance the symbol probabilities. The minimum PER is remarked in a red line.

We evaluate the simulation results with the estimation in terms of PER proposed in Sec. 3.4.2. Fig. 3.10 shows the comparison between the simulated result with the numerical. As shown, the proposed model, based on averaging the expected time interval matches with the simulation.

Fig. 3.10 shows the PER for different values of $\hat{\epsilon} = 0.02, 0.5, 1$ and SER_I. SER_I refers to the optimum symbol error rate achievable in a sub-interval T_I. We compare the results obtained by simulating the algorithm with the numerical results for assuming an average number $\overline{K}$ of subintervals per symbol. Additionally, in Fig. 3.11 we compare the performance of the algorithm, providing the PER estimation in an equivalent receiver with perfect synchronization over a minimum time interval, T_I and using a time interval wide enough to avoid the use of the algorithm.

The minimum time interval that ensures that transmitter and receiver will be synchronized until the end of the transmission is given by:

$$K_{no\ alg} = \lceil N_{bits}(\hat{N}_s + \epsilon) + 1/2 \rceil - \lfloor N_{bits}(\hat{N}_s - \epsilon) - 1/2 \rfloor \tag{3.14}$$

where N_{bits} stands for the number of bits that a packet contains. In this case, the interval $K_{no\ alg}$ is kept constant during all the reception. However this time interval must be kept larger to make sure that all he pulses during the transmission are received within the interval.

In this case, the PER is estimated by combining (3.1) and (3.13), with $r = K_{no\ alg}$. As shown in Fig. 3.11, the PER error provided with the adaptive frequency correction algorithm is

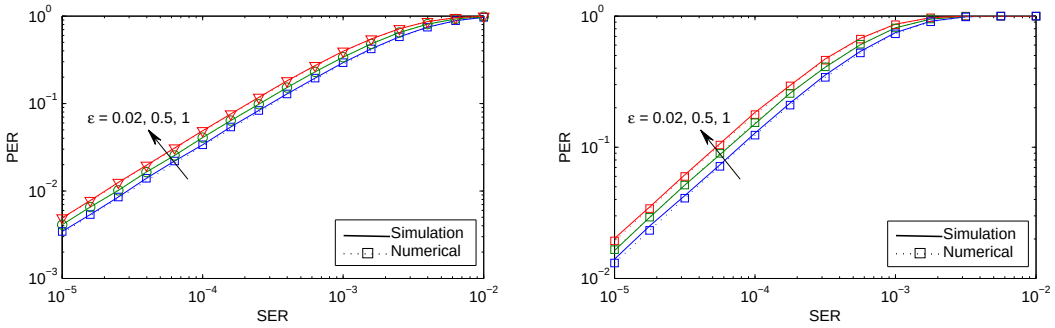

(a) $N_{bits} = 200$ bits (b) $N_{bits} = 800$ bits

Figure 3.10: PER estimation for different values of ϵ. Comparison between the numerical approximation and the simulation results

far better than using the smallest time interval that makes sure that the packet is successfully received, $K_{no\ alg}$ and the PER obtained approaches the optimum PER for a minimum time interval, supposing perfect synchronization, keeping the PER in the same order of magnitude.

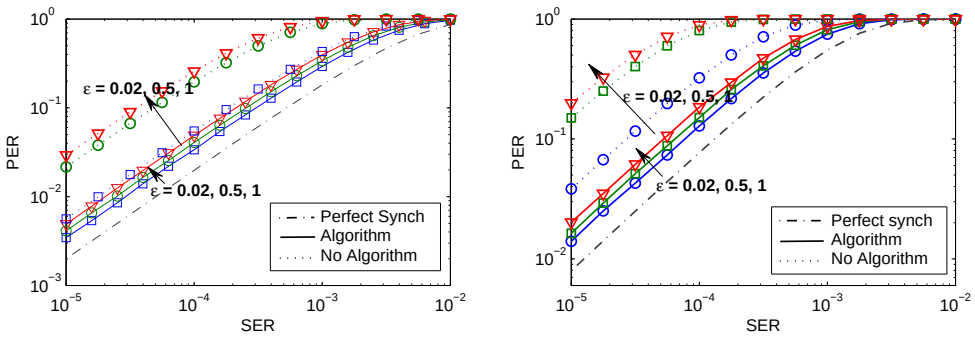

(a) $N_{bits} = 200$ bits (b) $N_{bits} = 800$ bits

Figure 3.11: PER estimation for different values of ϵ. Effect of the algorithm over the PER

3.5.4 Synchronization Preamble Metric

Long preambles reduce the $\hat{\epsilon}$ so the PER is reduced as well. However, considering that in order to satisfy the energy limitations, the total amount of energy to be transmitted is fixed, increasing the preamble implicitly means reducing the payload in $N_{synch}/P_{s=1}$. To observe this compromise, we introduce a normalized throughput defined as:

$$tput = \frac{(N_{bits}p - N_{synch}/P_{s=1})(1 - PER_{synch})p_{synch}}{N_{bits}(1 - PER_I)} \tag{3.15}$$

where N_{bits} is the total number of bits that the transmitter sends for each packet, $P_{s=1}$ stands for the probability of sending a "1", N_{synch} refers to the synchronization preamble length, PER_{synch} is the PER provided by the receiver using the synchronization preamble, PER_I refers to the PER provided by the equivalent receiver considering perfect synchronization and p_{synch} is the synchronization probability.

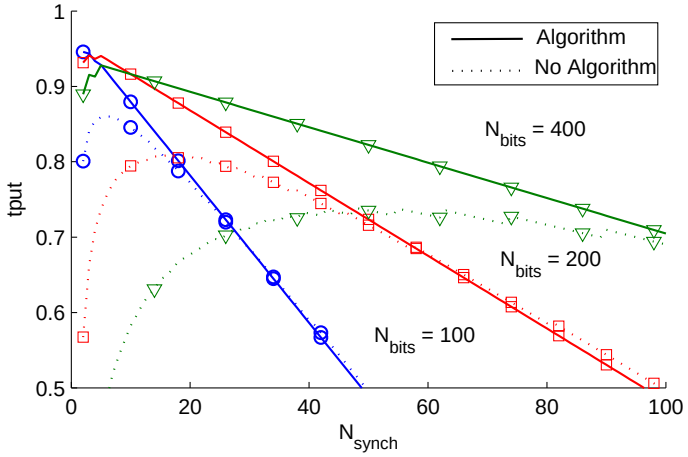

Figure 3.12: Normalized throughput as function of the preamble length.

Fig. 3.12 shows this normalized throughput for different distances and packet lengths. In order to compare the performance of the receiver, using the synchronization preamble and the adaptive frequency correction algorithm, we compare this normalized throughput with the normalized throughput obtained using only the frequency estimation and using the time interval fixed introduced in (3.14). As shown, the use of the algorithm reduces the necessity of long preambles providing a maximum in this normalized throughput for values below $N_{synch} < 10$ symbols.

3.6 Conclusions

In this chapter, we propose a novel symbol time estimation scheme for electromagnetic nanonetworks. This symbol time estimation scheme simplifies the basic structure of the transceiver, tailoring the ease integration of the TS-OOK modulation in nanodevices. Our solution provides an alternative to solve the lack of crystal oscillators in the nanoscale and avoids the use of PLL structures that are known for their inefficiency in carrierless modulations. We provide the probability of synchronization and packet error rate (PER) achievable in the channel for packets of few hundreds of bits using TS-OOK over the Terahertz channel. Finally, we explore the compromise between the number of bits needed to synchronize the symbol time between transceiver and receiver and the performance in the transmission, showing that using the proposed algorithm, we optimize the performance with short synchronization preambles of less than 10 bits.

Chapter 4

A Novel Symbol Time Synchronization Scheme for Electromagnetic Nanonetworks in the Terahertz Band

4.1 Introduction

In the previous chapters, the transceiver architecture and the symbol time synchronization scheme have been analyzed supposing that the receiver was able to detect an upcoming transmission. However, detecting that a nanodevice is sending a packet targeted to the receiver is challenging in nanonetworks. In this communication paradigm, the energy constraints limit the functionality and disable traditional synchronization schemes for WSN. In fact, we expect that nanodevices are able to send very short packets using a rate of few packets every few seconds. This low traffic implies that sending packets with synchronization purpose only adds a very high overhead. Additionally, since the packet rate is very low, the synchronization among nanodevices is expected to be lost from one packet to another.

In this chapter we analyze the communication from the receiver's perspective. This receiver must be able to efficiently detect when a new transmission is about to be started to successfully decode the packet. To detect a new transmission, we propose the use of a wake-up receiver. A wake-up receiver is an asynchronous synchronization scheme where the transmitter sends a wake-up signal to a sleeping receiver [77]. In this chapter we explore this synchronization scheme by proposing a burst of pulses as a wake-up signal.

Fig. 4.1 shows the relationship between this wake-up receiver and the transceiver presented in Chapter 2. Our main contributions can be summarized as follows:

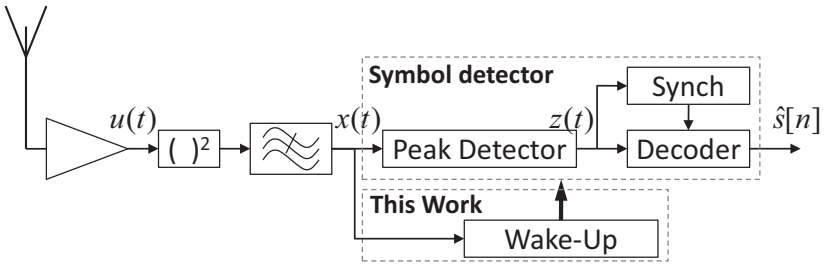

Figure 4.1: Receiver block diagram with Wake-Up module.

- We introduce the wake-up receiver for EM nanonetworks based on a pulse burst wake-up signal.
- We propose an orthogonal burst to reduce the interferences between neighboring nodes.
- We analize the probability of detecting new transmissions, as well as the energy consumption of this synchronization scheme.

The rest of this chapter is organized as follows. In Sec. 4.1.1, we describe the network architecture. In Sec. 4.2, we describe the wake-up receiver architecture. In Sec. 4.3, we describe the orthogonal burst preamble. In Sec. 4.4, we validate the wake-up receiver and evaluate its performance. In Sec. 4.5, we conclude the work presented in this chapter.

4.1.1 Nanonetwork Architecture

In contrast to the previous Chapters, where the nanodevice has been analyzed in a point to point topology, the synchronization among nanodevices implies a specific network architecture. We consider the nanonetwork architecture introduced in [1] which also provides the interconnection between the nano- and micro- worlds as it is shown in Fig. 4.2.

As shown in Fig. 4.2, this architecture is composed by the following entities:

- **Nano-nodes:** We expect that each nanodevice mentioned in this work behaves as a nano-node of the network. These are small devices which are able to perform simple tasks such as sensing. These nanodevices densely deployed over the nanonetwork and communicate among them by using the TS-OOK modulation scheme. Additionally, they have routing capabilities to forward the packets from other nano-nodes to the destination. As an example in the medical field, these nano-nodes can be the sensors capable detect viruses or possible health problems which are deployed in an intra-body nanonetwork.
- **Nano-routers:** We consider that among all the nanodevices, some of them are deployed for relaying packets only. Since the communication among nanodevices is expected to be the post power consuming process, these nano-devices are expected to be bigger in

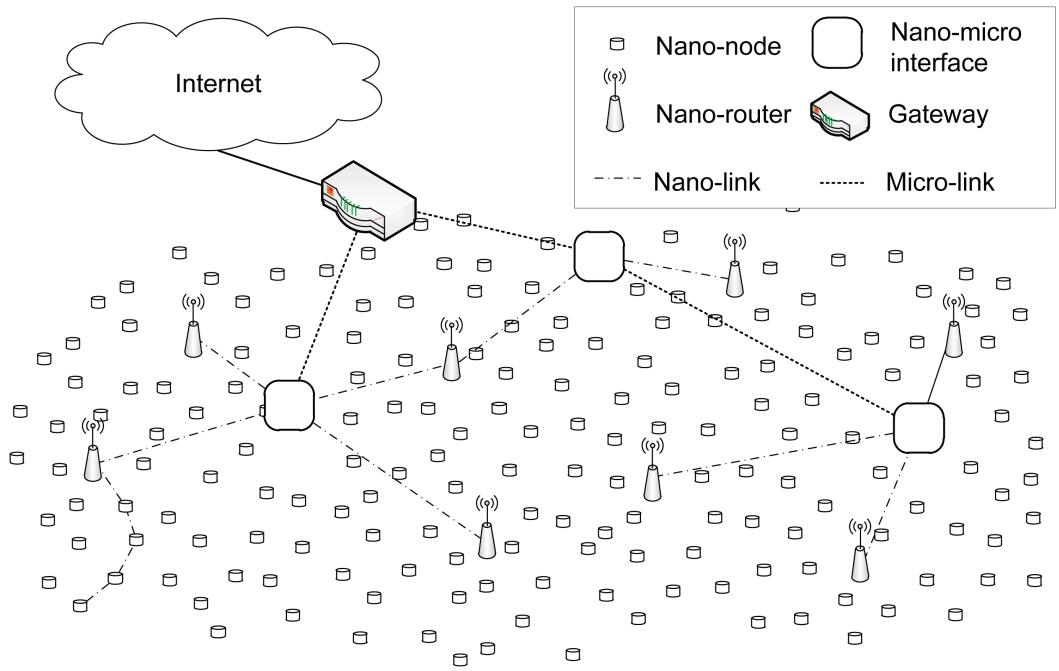

Figure 4.2: Network architecture for EM Nanonetworks.

size than other nanodevices and enables transmission in longer distances. Moreover, we expect these nano-devices to manage and to coordinate a group nano-nodes close to the nano-router. As an example in the medical field, these nano-routers coordinate and forward the sensed data to be collected.

- **Nano-micro Interface:** These nano-micro interfaces enable the interconnection of both nano and micro worlds. Thus, these interfaces can communicate to other nodes by using the TS-OOK modulation over the Terahertz band and also by using conventional communication schemes. As an example in the medical field, these interfaces can be a patch which is able to communicate with a cell phone to forward the data to the healing center.

- **Gateway:** These macro-devices enable the human interaction with the nanonetwork. Additionally, these gateways enables the interconnection of these nanonetwork with conventional networks. As an example, a gateway can be implemented with a cell phone which reads the sensed data from a nano-micro interfaces and forwards the data to the healing center.

In our work, we assume that the network is balanced in terms of traffic and resources so every node in the nanonetwork is supporting the same traffic and is operating with the same properties and constraints than the other nodes of their same category.

In particular, we assume that a nanodevice or nano-node is able to generate traffic at a rate λ_{packet} and forwards a traffic relayed from neighboring nanodevices λ_{relay}. Thus, we have

that the actual traffic that a nanodevice is sending to the network can be expressed as:

$$\lambda_{Tx} = \sum_{i=0}^{K} (\lambda_{packet} + \lambda_{relay}) = (M+1)\lambda_{packet} \frac{1-(1-p_{success})^{K+1}}{p_{success}} \tag{4.1}$$

where K is the maximum number of retransmissions, λ_{packet} stands for the packet generation rate, λ_{relay} refers to the traffic relayed from other nodes, which we consider to be equal to $M\lambda_{packet}$ and $p_{success}$ is the success probability in the transmission of a packet which is a function of the packet error rate and probability of synchronization. M refers to the average number of hops that a packet has to go through to reach its destination.

4.2 The Wake-Up Receiver for EM Nanodevices

The energy that a nanodevice can store is comparable to the energy needed to send a few packets of information. This energy limitation makes the device to switch off and more likely after the exchange of information with neighboring nodes. When the nanodevice has again enough power, it is switched on and it tries to reincorporate into the network. This situation in nanosensor networks makes the nodes to frequently lose any synchronization.

Many protocols for synchronization in wireless sensor networks have been proposed in the previous years. Existing specific carrier sensing protocols for sensor networks, such as SMAC [78] and variations or improvements [79, 80], do not apply in carrierless communications the nanonetworks paradigm.

This context leads to explore different synchronization schemes. In particular, we propose to use a Wake-Up receiver synchronization scheme. In this synchronization scheme, the energy used to sense the channel every a certain time is spread in time. Fig. 4.1 shows a comparison between both synchronization schemes. In then upper part, the receiver switches on periodically and it tries to detect a synchronization preamble, while in the Wake-Up scheme, the receiver is always listening to the channel.

To enable this synchronization, the listening energy in the Wake-Up receiver must be much lower than in the previous case. To reduce this energy, the wake-up signals must be easier to detect than normal packets. This synchronization scheme is considered asynchronous, which means that the transmitter will just wake-up the receiver when there is information to transmit, otherwise the receiver is in a sleep mode. Therefore, we solve two main issues in synchronization:

- *Symbol time estimation:* In Chapter 3 we discussed the possibility of having different frequencies. Thus, before detecting the synchronization preamble, nanodevices should synchronize. However, the receiver node does not synchronize with the transmitter until it detects a new transmission.

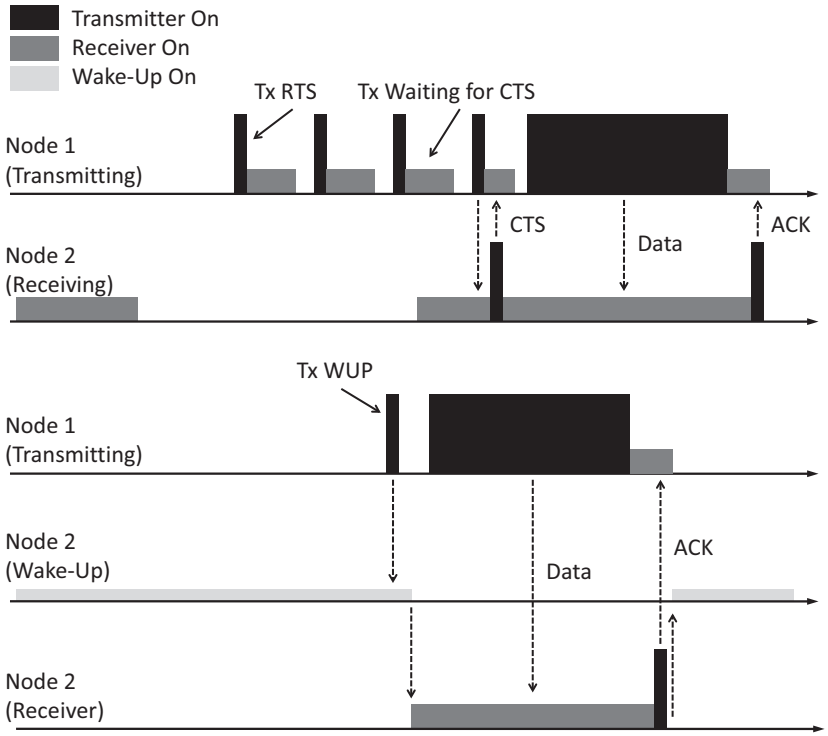

Figure 4.3: Comparison of protocol-based duty cycling and wake-up.

- *Asynchronous:* A delay of a few tens of nanoseconds in synchronous synchronization schemes implies that the receiver has lost at least half of the packet.

4.2.1 Burst Detection and Start of Packet Transmission

To detect a new transmission, the transmitter device must send a wake-up signal to the receiver. This signal must be easier to decode, so the power in standby can be significantly reduced compared to the listening power and it must be different to any other signal to avoid false alarms.

Authors in [77, 81] propose different alternatives to implement wake-up transceivers. In particular, to differentiate between the Wake-Up signal and the data transmission, in [77], authors use a second frequency to wake-up the receiver. This difference between wake-up signal and data packets guarantees that nodes in the sleeping state are not waken-up during the communication among neighboring nodes. To implement this wake-up transceiver, they propose a power detector matched to this second frequency which activates the receiver if the amount of power detected is above a threshold.

In contrast, the TS-OOK modulation scheme is defined as a carrierless broadband modulation that uses the whole Terahertz band by transmitting very short pulses. Because of this, the use of orthogonal frequencies does not apply for the detection of a new transmission. Additionally, while very short pulses can be efficiently generated and radiated [66], the generation of a tone in the Terahertz band requires a high power oscillator.

For this, the difference between wake-up signals and information cannot be defined in the frequency domain, but in the time domain. We propose a pulse burst as wake-up signal. This is a short and fast burst of N_B pulses during a time lower than the symbol time,$T_B < T_S$. If the burst time is lower than the symbol time, we observe that, on the one hand, a new transmission will not probably interfere any other existing transmission in more than one symbol, while on the other hand, an existing transmission cannot be interpreted as a burst for a new transmission.

The Burst is a train of pulses sent to a higher rate than the packet rate. In this way, the channel can still be modeled as error probability of detecting a pulse p_d as we have previously determined in Chapter 2. To provide robustness in reception, we propose to consider a successful detection if any N_b pulses among the total N_B are successfully detected.We propose to model the burst of pulses as N_B independent pulses with error probability p_d. Then, the probability of detecting a burst, P_D, with at least N_b pulses is given by:

$$P_D = \sum_{i=0}^{N_B - N_b} \binom{N_B}{N_b + i} (1 - p_d)^{N_b + i} p_d^{N_B - N_b - i}. \tag{4.2}$$

Finally, although the optimum error probability p_d can be obtained as shown in Chapter 2, we assume that the actual error probability is worse in at least one order of magnitude, due to this power detection is expected to be implemented with passive circuits to reduce power consumption.

4.2.2 Noise and Interference Model

The noise collected by the antenna can affect the detection only if the noise level is above the threshold of detection. When the noise signal is strong enough the receiver interprets the noise as a pulse. Considering that the receiver is working to a fixed frequency f_0, we assume that the probability of detecting a pulse during one period $T = 1/f_0$ is given by p_0. This probability has been already presented in Chapter 2 and it depends on the time interval T of observation. When T is large enough to uncorrelate consecutive periods, this noise can be modeled as a poisson arrival with:

$$\lambda_n = p_0/T. \tag{4.3}$$

Similar to the pulse detection, the probability of decoding noise as a possible pulse is also considered worse in at least one order of magnitude to reduce the power consumption.

Neighboring nodes also provide errors in the detection of new bursts. The interference of neighboring nodes can be modeled as a Poisson process given by:

$$\lambda_i = N\lambda_{Tx} = A\rho\lambda_{Tx}. \tag{4.4}$$

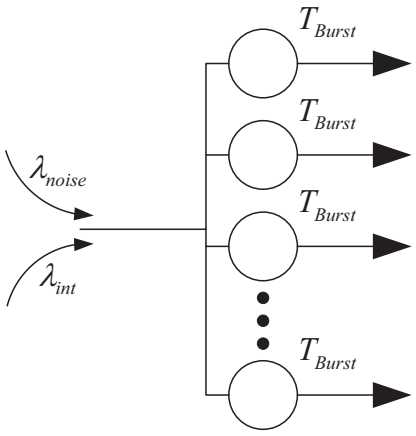

Figure 4.4: M/D/c/c equivalent model for noise and interferences.

where λ_{Tx} is the data that a single node is sending, $N = A\rho$ refers to the number of nodes, A stands for the area that the device can reach and ρ is the node density. λ_{Tx} is obtained from (4.1)

Considering interferant pulses and noise as poisson arrivals, we model the Wake-Up module in presence of noise and interference as a M/D/c/c queue with N_B servers with a service time T_B. The input is the addition of both noise and interference traffic. Fig. 4.4 shows the queue model proposed for the wake-up module.

The parameter of interest must refer to the number of pulses received in a time T_B. This can be interpreted as the number of users that are currently in the queue or active servers, since there is no queue in the model. The probability of having n active servers is given by:

$$p_n = \frac{(\lambda T_B)^n/n!}{\sum_{k=0}^{N_B}(\lambda T_B)^k/k!} \tag{4.5}$$

where $\lambda = \lambda_n + \lambda_i$ are the arrivals provided by the noise and interference, T_s refers to the service time and N_B stands for the total number of servers.

As commented in Sec. 4.2.1, to provide more robustness to the receiver and be able to detect burst even if not all of the pulses have been detected, a minimum of N_b detected pulses are needed to switch-on the receiver. In the queue model, which means that as long as there are a minimum of N_b servers active, the receiver is waken up. Thus, the probability of having N_b or more pulses in the system is provided by:

$$p_{fa} = \sum_{n=N_b}^{N_B} p_i. \tag{4.6}$$

As can be expected, short bursts increase the probability of detecting false alarms, defined as detecting a new burst due to noise or interferences, while large bursts will increase the packet overhead and energy needed for the transmitter to send the packet.

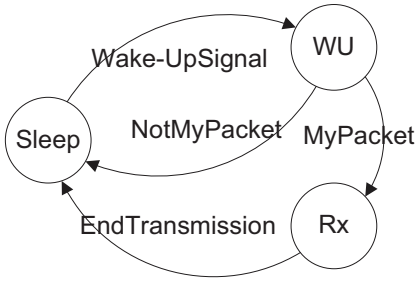

Figure 4.5: Simplified receiver state-machine.

4.3 Orthogonal Burst Preamble

After detecting a burst, the receiver has to decide whether to wake up or not. In the nanonetworking paradigm, we assume that the energy constraints make the packet length to be around few hundreds of bits, as commented in Sec.1.2.4. The reduced packet length makes the energy for waking-up, synchronizing transmitter and receiver and detecting if this nanodevice is the target for the reception of this packet to be comparable to the energy that a nanodevice needs to successfully receive a packet.

To help the nanodevice in its decision, we propose the use of a second burst. Once the receiver has detected the first wake-up burst, the receiver switches to a wait state which mainly lets the receiver to switch off the radio until a second burst is about to come, the time between bursts is referred as T_i sec. Then the receiver waits a time T_{out} where the pulse is expected to arrive. If the receiver detects within T_{out} a new burst, it accepts the reception and proceeds to synchronize the frequencies between the transmitter and receiver and to receive the packet. Otherwise, it discards the new packet detection and it switches back to the wake-up state. This stateflow diagram is shown in Fig. 4.5.

The time T_{out} is related to the accuracy between clocks and it is assumed to be an external parameter which will be provided by future technologies used to implement the timing schemes in the nanodevices. The available number of T_i is conditioned by T_{out}, the more accuracy, the more different T_i we can have. It is also conditioned by complexity. Different T_i must be stored in memory. For this we consider that in a nanonetwork there is a total of K different T_i.

Using a second burst to help the receiver in the decision provides some advantages. Firstly, it reduces the probability of false alarm. In fact the probability of detecting a burst made of noise or random interferences in a very short time, in this case T_{out} is highly improbable. Secondly, it allows the receiver to have shorter bursts, while providing the same performance. This fact will also simplify the design of these nanodevices. Additionally, the time between bursts can be also used to do a first frequency estimation.

When the receiver switches on to try to detect the second burst after a time T_i. It is implicitly performing a dot product between the time between bursts and the expected time

in the receiver. We refer this time between bursts as burst address. We can express this burst address as a K-dimension vector composed by $\boldsymbol{a} = (0, \cdots, 0, 1, 0, \cdots, 0)$ where each component indicates a pulse after a time T_i since the first burst with $i \in K$. The dot product between the burst addresses $\boldsymbol{a}^r \cdot \boldsymbol{a}^t$ where $\boldsymbol{a}^t$ refers to the targeted burst address and the $\boldsymbol{a}^r$ stands for the burst address of the receiver. In this case, since the burst addresses are composed by all zeros and just a one, when both addresses match, the result of the dot product is "1" so the receiver will receive the upcoming packet, otherwise the receiver will switch back to the standby.

We can distinguish between two possibilities, if the number of available burst address, K, is greater or equal than the neighboring nodes in the network, each neighbor can be identified with a different addresses so, first of all, the receiver is only switched on when a packet from a neighboring node is headed for him and, secondly, there is no need of additional MAC address to identify different neighboring nanodevices. However, if the number of available burst addresses, K, is lower than the neighboring nodes in the network, the recevier is also switched on when a packet is not headed for him. In this case, there is a probability of not acceptance, p_{arej}, which models the probability of rejecting a packet which is not sent to the receiver. This is given by:

$$p_{rej} = \frac{1}{K}\frac{N-K}{N-1} \tag{4.7}$$

where N is the number of neighboring nanodevices plus the nanoreceiver and K refers to the maximum number of different burst addresses. In this case, where the K is lower than the total number of nanodevices in a unitary area, N, additional MAC address is needed to univocally identify the target nanodevice. Either way, protocols in the above layers must be defined to efficiently distribute the available addresses.

Finally, notice that there is no reason why this second burst should have the same length, N_{B2}, than the first burst. In fact, the first burst length, N_B, is fixed to avoid that noise and interference during the time between packets could be interpreted as a new burst. N_{B2} must be fixed to reduce this false alarms just during T_{out}. While the time between packets is expected to be in the order of seconds, T_{out} is expected to be in the order of the symbol time.

4.4 Performance Evaluation

4.4.1 System Model

- The path-loss and noise in the Terahertz band are computed by using the models introduced in [4]. A standard medium with 10% of water vapor is considered.
- The transmitter encodes logical "1" by using 1 pJ 100 femtosecond-long gaussian pulses. The second time-derivative of the gaussian pulse is supposed to be detected in the receiver. The logical "0" is transmitted as silence.

- The symbol probabilities are considered equal for the logical "1"s and "0"s. $p_{s=0} = p_{s=1} = 0.5$.
- The SER and the error probabilities for the logical "0" and "1" are estimated by using the receiver architecture of Chapter 2. However, if the SER is not specified, we consider $SER = 10^{-4}$.
- A packet is limited to a few hundreds of pulses. Thus we do not correction algorithms. Thus, the packet length is set to a few hundreds of bits and a single error in the transmission of a packet makes the packet to be unsuccessfully decoded.
- When the receiver is in standby, the probability of detection of a pulse is reduced in a factor α. This is due to lower the power consumption constraints.
- The power consumption in the receiver depends on the state. We consider a power consumption $P_{sleep} = 1pW$ for the sleeping state, an energy consumption of 1 pJ per pulse in the burst during the Wake-Up state, Finally, an energy consumption of 0.7 pJ per pulse during the reception of the pulse.

4.4.2 Protocol Description

To evaluate the functionality of this wake-up receiver. We propose the use of a simple synchronization protocol built on top of the ALOHA protocol. The ALOHA is a well studied protocol that provides a good performance for low traffic networks, which is the case of nanonetworks where there is low traffic generation and the packet length is very short. Additionally, the use of the TS-OOK provides almost orthogonal channels which significantly reduce the collision between packets.

This protocol consists of three processes and it is explained as follows:

Wake-Up Process:

The transmitter decides when a the packet must be sent. Before sending the packet, the transmitter sends two bursts with a distance between bursts of T_i seconds. The time T_i^s between bursts is set according to the destination nanodevice. For this, we assume that burst addresses are previously distributed over the nanodevices. The receiver, is in the wake-up state until it detects the first burst, it waits a time T_i^r for the second burst to arrive. If the second burst arrives while the receiver is reading, the receiver accepts the packet and it starts receiving the packet. Otherwise, the receiver switches back to the wake-up state.

Time and Frequency Estimation Process:

Transmitter and receiver are not synchronized in time. Pulse-based communications need an estimation of the time of arrival. As we showed in Chapter 3, this time and frequency

estimation scheme can be performed by using a very short preamble of less than 10 bits, by affecting the symbol error rate in a factor $r = 1.36$.

Data Transmission Process:

The transmitter sends the packet to the receiver by using the TS-OOK modulation scheme. The receiver uses the adaptive algorithm provided in the Chapter 2 to follow the time variations and non-idealities. We do not consider any channel codification thus, a packet is successfully received as long as there is no any error during the reception.

Burst Acknowledgement Process:

If the packet has been successfully received, the receiver sends an acknowledge packet to the transmitter nanodevice. The shortest packet that a nanodevice can send is just a burst of pulses. For this, a pulse burst is sent to acknowledge the transmission. We refer this pulse burst as Burst Acknowledgement (BACK). To avoid that third nanodevices can wake up once they listen to the BACK, this pulse burst must be shorter than the needed to start a transmission so a neighboring receiver does not interpret the burst as a wake-up signal. The transmitter after sending the packet waits for the BACK signal. If the transmitter does not detect any burst, the transmitter calculates a back-off time and, after that, if the number of retransmissions have not exceeded the maximum number, it retransmits the packet again.

4.4.3 False Alarm Probability

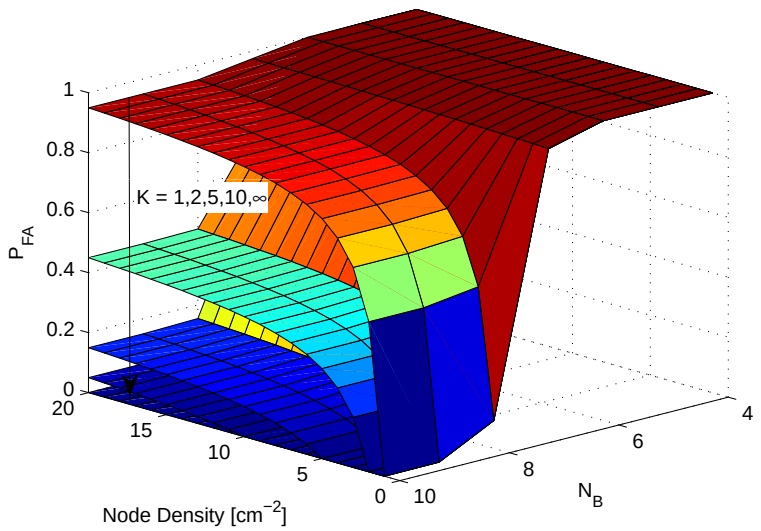

Figure 4.6: Probability of detecting false alarm in terms of the number of users and N_B.

We define a false alarm as detecting noise or interference as a wake-up signal. The false alarm probability mainly depends on the number of pulses of the first burst. The more pulses

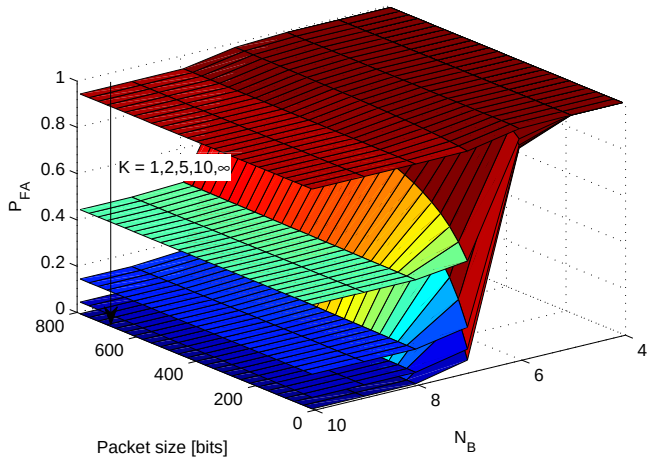

Figure 4.7: Probability of detecting false alarm in terms of the packet length and N_B for 20 neighboring nodes.

needed to activate the receiver, the more robust the receiver is. Thus, the use of short bursts increase the false alarm probability while long bursts increase the overhead and the minimum energy needed to transmit a packet.

In Fig. 4.6 we show this probability in terms of the node density and the burst length for different values of the maximum number of orthogonal bursts. Notice that $K = \infty$ refers to having more orthogonal burst preambles than possible interfering nodes. This probability refers to the probability for a new transmission detected to not being a packet targeted to the nanodevice. As shown, when the burst length is very short, the system cannot differentiate between burst preambles and noise. In this case, the receiver will constantly be interpreting noise as new packets which has a very strong effect in the energy consumed by the nanodevice.

Alternatively, when the burst length is large enough, eight or more pulses, the effect of the noise is neglected and the receiver is mainly affected by the interferences and by the burst . In this case, as shown, the use of orthogonal burst preamble significantly reduces this false alarm probability. This is because the receiver is able to notice before the reception starts if the packet is targeted to itself or it is targeted to a different node.

In Fig. 4.7, we show the effect that the packet size has over the false alarm probability also for different values of the maximum number of orthogonal bursts. As shown, the smaller the packet is, the lower false alarm probability we obtain. This is because using a fixed information generation rate, lower the packet length means lower the time between packets which reduces the probability of receiving false alarms between packets. However, small packet lengths are heavily affected by overhead significantly lowering the energy efficiency.

4.4.4 Loss Probability

We define the loss probability as the probability of not receiving a packet because the receiver was not listening to the channel in the sleep state. In this loss probability we only consider the effect that the protocol with the orthogonal burst preambles has over this error probability.

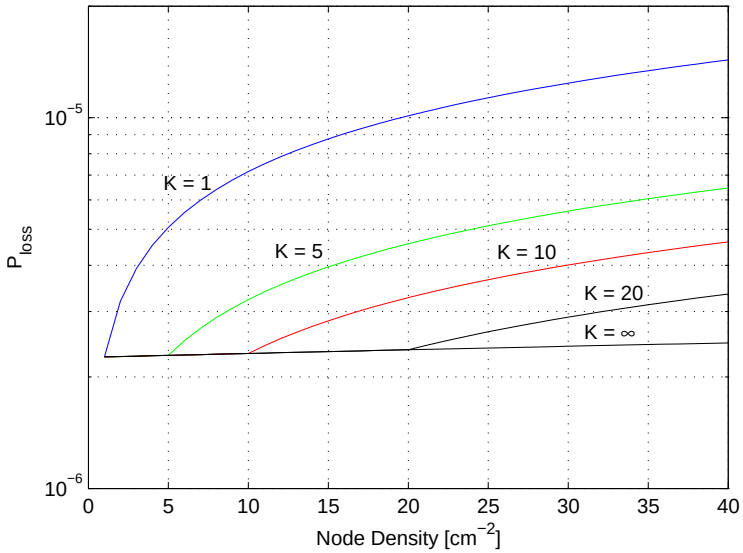

Figure 4.8: Probability of finding the receiver handling a packet in terms of the node density for different maximum number of burst preambles.

As shown in Fig. 4.8 the loss probability can be kept almost constant as long as the maximum number of orthogonal burst preambles is kept greater than the maximum nodes that can interfere. However, due to the low traffic generated by the network, this probability is still very low, which confirms that collisions are very unlikely to happen. In the eventual analysis, this loss probability will mainly influenced by the time the devices is switched of due to lack of energy.

4.4.5 Energy Consumption in Reception for the Wake-Up Based Transceiver.

The main aim of the Wake-Up module is to lower the energy consumption of the block as well as enabling an asynchronous synchronization protocol between nanodevices. Each state of the stateflow machine has a power associated. The energy per bit has been evaluated by the energy used in each one of the states between two successful transmissions. This way, the energy per bit also counts the energy wasted in the wake-up state and in the burst state.

We have modeled the energy consumption of the receiver in terms of the stateflow shown in Fig. 4.5. Thus, we have considered the following parameters for the energy consumption estimation:

- The power consumption while the nanodevice is in standby is 0.7 pW.

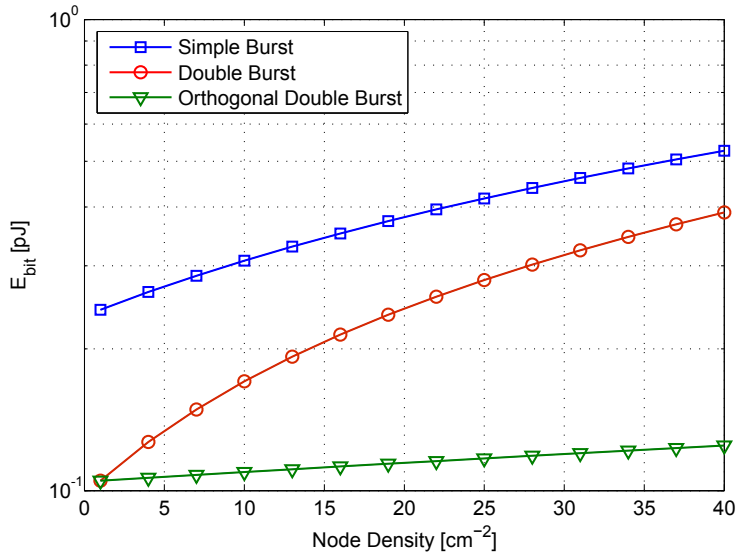

Figure 4.9: Energy per bit spent by the receiver in terms of the node density for different maximum number of burst preambles.

- The energy consumption in the reception of the second burst is function of the number of pulses that the burst contains, N_{B2}. This is 0.1 pJ per pulse.

- The energy consumption for the symbol time estimation is depends on the number of synchronization burst preamble and it is higher than the energy per pulse in reception. This is 0.25 pJ per pulse.

- The energy consumption in reception is fixed to 0.1 pJ per pulse plus the energy consumed to send the BACK packet in case of a successful reception. The energy needed to send the BACK is set to 4 pJ.

Fig. 4.9 shows the energy per bit needed to receive a successful packet in case of a single burst, a double burst and an orthogonal double burst. As shown, In case of using a single burst, the receiver wakes up every time it receives noise or interferences, so the energy per bit is increased. In case of using a second burst, the receiver wakes up every time it detects a new transmission. This fact makes the receiver to wake up and waste energy for packets that are not targeted to it. Finally, the use of orthogonal burst preambles helps the receiver to decide when it has to wake up. In this case, although the receiver detects new transmissions, the receiver is able to detect if the receiver is the target of the packet or not. In case the receiver is not the target, it is able to reject the packet without waking up all the receiver. This fact provides an almost constant energy dependence with the node density.

4.5 Conclusions

In this chapter, we propose a novel synchronization scheme for electromagnetic nanonetworks. This synchronization scheme simplifies the basic structure of the transceiver, tailoring the ease integration of the TS-OOK modulation in nanodevices. Our wake-up receiver proposes an orthogonal burst preamble to enable asynchronous communication and to detect new transmissions. We provide a model for the signal and noise in the receiver. We evaluate the model in terms of probability of false alarm and in terms of energy consumption in the receiver. The results show that despite its simplicity, this novel wake-up receiver enables the communication among nanodevices and provides an almost node density independence in case the orthogonal burst preamble is being used.

Chapter 5

Open Issues and Conclusions

5.1 Open Issues

Wireless Nanosensor Networks is a novel field which is attracting the attention of scientists from different backgrounds. In fact nanotechnology and nanonetworks are providing very promising results but opening up several challenges.

After this work, there is a long way to pave before nanonetworks can become a real communication paradigm. Regarding this work, we foresee the inclusion of the transceiver architecture parameters into a networking simulator. Including the symbol time estimator and more important, the wake-up synchronization scheme. With the inclusion of these parameters and the energy constraints, we envision a further study and validation of the results of this work, as well as the development novel networking protocols for EM Nanonetworks built on top of this architecture.

Additionally, some other work must be done. Regarding the nanodevice, the scientist and engineering community needs a deeper study on nanomaterials and nanotechnology to provide a set of tools for the development of novel circuits to implement future nanodevices. Alternatively, in the field of communications, the graphene-based nano-antenna introduced in [49] must be implemented and tested over the Terahertz channel. Moreover, the Terahertz channel must also be characterized and studied for short path communications.

5.2 Conclusions

This thesis has studied the bridge between the nanodevice and the nanonetwork. The main purpose of this work has been to provide a model to use in further simulations or future implementations that will enable the communication of these nanodevices inside the network.

Firstly, we propose a novel transceiver architecture. This architecture simplifies the basic structure of the transceiver, tailoring the easy integration of impulse-based modulations, such

as the recently introduced TS-OOK modulation for nanodevices. We mathematically describe the probability density functions of the received symbols and validate the results through simulation. We provide the symbol error rate estimation in the Terahertz band as function of the distance. Moreover, we provide a post-simulation model to simplify the estimation of the symbol error rate over the channel. The results show that, in the Terahertz channel, the novel transceiver architecture for nanodevices outperforms existing impulse-radio based transceivers reducing the symbol error rate and increasing the transmission distance. Moreover, we show that the proposed nano-transceiver can also support bitrates of up ot terabits per second for distances in the order of tens of millimeters using very simple modulation schemes.

Secondly, we study the effect of non-idealities in the timing scheme of nanodevices, which are related to the available energy and low cost. We propose a novel symbol time estimation scheme for electromagnetic nanonetworks. This symbol time estimation scheme simplifies the basic structure of the transceiver. Our solution provides an alternative to solve the lack of crystal oscillators in the nanoscale. We provide the probability of synchronization and achievable packet error rate in the channel for packets of few hundreds of bits. Finally, we explore the compromise between the number of bits needed to synchronize the symbol time between transceiver and receiver, showing that this preambles can be implemented with less than 10 pulses.

Finally, we observe that all this work is only possible if the receiver is able to detect when a new transmission is headed for itself. We propose a novel synchronization scheme for electromagnetic nanonetworks. This synchronization scheme is able to detect a new transmission from noise and interferences. To reduce the false alarm probability, we propose the use of orthogonal bursts and we explore the effect of this synchronization scheme over the energy consumption in the receiver.

We foresee this work as bridging the nanonetwork and the nanodevice. In fact, the future inclusion of this model in network simulators will help the study of nanonetworks and it will condition the design of future networking protocols designed on top of this architecture.

Appendix A

Acronyms

CNT Carbon Nanotube

CNT-FET CNT Field-Effect Transistor

EM Electromagnetic

FET Field-Effect Transistor

GNR Graphene Nanoribbon

GFET Graphene Field-Effect Transistor

IR-UWB Impulse Radio Ultra-Wide-Band

MEMS Micro-Electro-Mechanical System

MWNT Multi-walled Nanotube

NEMS Nano-Electro-Mechanical System

OLC Onion-Like-Carbon

PLL Phase Locked Loop

PER Packet Error Rate

PPM Pulse Position Modulation

PAM Pulse Amplitude Modulation

SER Symbol Error Rate

SET Single Electron Transistor

STNO Spin Torque Nano-Ocillator

SWNT Single-walled Nanotube

TS-OOK Time Spread On-Off Keying

WSN Wireless Sensor Network

WNSN Wireless NanoSensor Network

ZnO Zinc Oxide

Bibliography

[1] I. F. Akyildiz and J. M. Jornet. Electromagnetic wireless nanosensor networks. *Nano Communication Networks (Elsevier) Journal*, 1(1):3–19, March 2010.

[2] Josep Miquel Jornet and Ian F. Akyildiz. Graphene-based nano-antennas for electromagnetic nanocommunications in the terahertz band. In *Antennas and Propagation (EuCAP), 2010 Proceedings of the Fourth European Conference on*, pages 1 –5, April 2010.

[3] Yu-Ming Lin, Alberto Valdes-Garcia, Shu-Jen Han, Damon B. Farmer, Inanc Meric, Yanning Sun, Yanqing Wu, Christos Dimitrakopoulos, Alfred Grill, Phaedon Avouris, and Keith A. Jenkins. Wafer-scale graphene integrated circuit. *Science*, 10:1294–1297, 2011.

[4] J. M. Jornet and I. F. Akyildiz. Channel capacity of electromagnetic nanonetworks in the terahertz band. In *Proc. of IEEE International Conference on Communications, ICC*, pages 1–6, May 2010.

[5] J. M. Jornet and I. F. Akyildiz. Information capacity of pulse-based wireless nanosensor networks. In *to appear in Proc. of the 8th Annual IEEE Communications Society Conference on Sensor, Mesh and Ad Hoc Communications and Networks (SECON), Salt Lake City, Utah, USA*, June 2011.

[6] I. F. Akyildiz, W. Su, Y. Sankarasubramaniam, and E. Cayirci. Wireless sensor networks: a survey. *Computer Networks (Elsevier) Journal*, 38(4):393 – 422, March 2002.

[7] Norio Taniguchi. On the basic concept of 'nanotechnology'. *Proc. ICPE Tokyo*, 2:18–23, 1974.

[8] Robert Curl Jr. Indian craftsmen, artisans used nanotechnology 2000 years ago. 95th Indian Science Congress.

[9] S. Srinivasan and S. Ranganathan. India's legendary 'wootz' steel: an advanced material of the ancient world. National Institute of Advanced Studies and Indian Institute of Science.

[10] Christofer Hierold, Alain Jungen, Christoph Stampfer, and Thomas Helbling. Nano electromechanical sensors based on carbon nanotubes. *Sensors and Actuators A: Physical*, 136(1):51 – 61, 2007.

[11] Jordi Riu, Alicia Maroto, and F. Xavier Rius. Nanosensors in environmental analysis. *Talanta*, 69(2):288 – 301, 2006.

[12] Yaping Dan, Ye Lu, Nicholas J. Kybert, Zhengtang Luo, and A. T. Charlie Johnson. Intrinsic response of graphene vapor sensors. *Nano Letters*, 9(4):1472–1475, 2009.

[13] Bo Zhang and Tianhoung Cui. An ultrasensitive and low-cost graphene sensor based on layer-by-layer nano self-assembly. *Applied Physics L*, 98:073116, 2011.

[14] Ulrike Tisch Peng Gand and Hossam Haick. Detection of nonpolar molecules by means of carrier scattering in random networks of carbon nanotubes: Toward diagnosis of diseases via breath samples. *American Chemical Society*, 9(4):1362–1368, 2009.

[15] Padmavathy Tallury, Astha Malhotra, Logan M Byrne, and Swadeshmukul Santra. Nanobioimaging and sensing of infectious diseases. *Advanced Drug Delivery Reviews*, 62(4-5):424–437, March 2010.

[16] F. Schedin, A. K. Geim, S. V. Morozov, E. W. Hill, P. Blake, M. I. Katsnelson, and K. S. Novoselov. Detection of individual gas molecules adsorbed on graphene. *Nature Materials*, 6(9):652–655, 2007.

[17] C. Roman, F. Ciontu, and B. Courtois. Single molecule detection and macromolecular weighting using an all-carbon-nanotube nanoelectromechanical sensor. In *4th IEEE Conference on Nanotechnology*, pages 263–266, August 2004.

[18] P. Kim. Toward carbon based electronics. In *IEEE Device Research Conference*, June 2008.

[19] Phaedon Avouris. Carbon nanotube electronics and photonics. *Physics Today*, 62(1):34–40, January 2009.

[20] Chanda Ranjit Yonzon, Douglas A. Stuart, Xiaoyu Zhang, Adam D. McFarland, Christy L. Haynes, and Richard P. Van Duyne. Towards advanced chemical and biological nanosensors - an overview. *Talanta*, 67(3):438 – 448, 2005.

[21] Chunyu Li, Erik T. Thostenson, and Tsu-Wei Chou. Sensors and actuators based on carbon nanotubes and their composites: A review. *Composites Science and Technology*, 68(6):1227 – 1249, 2008.

[22] Rodrigo Fernandez-Pacheco, J. Gabriel Valdivia, and M. Ricardo Ibarra. Magnetic nanoparticles for local drug delivery using magnetic implants. *Methods in Molecular Biology*, 544:559–569, June 2009.

[23] Yanqing Wu, Yu ming Lin, Ageeth A. Bol, Keith A. Jenkins, Fengnian Xia, Damon B. Farmer, Yu Zhu, and Phaedon Avouris. High-frequency, scaled graphene transistors on diamond-like carbon. *Nature*, 472:74 – 78, 2011.

[24] Guanglei Cheng, Pablo F. Siles, Feng Bi, Cheng Cen, Daniela F. Bogorin, Chung Wung Bark, Chad M. Folkman, Jae-Wan Park, Chang-Beom Eom, Gilberto Medeiros-Ribeiro, and Jeremy Levy. Sketched oxide single-electron transistor. *Nature Nanotechnology*, 1:1748–3387, 2011.

[25] Antonio Di Bartolomeo, Mohamed Rinzan, Anthony K Boyd, Yanfei Yang, Liberata Guadagno, Filippo Giubileo, and Paola Barbara. Electrical properties and memory effects of field-effect transistors from networks of single- and double-walled carbon nanotubes. *Nanotechnology*, 21:115204, 2010.

[26] M. Dragoman and D. Dragoman. The carbon nanotube radio. In *Semiconductor Conference, 2008. CAS 2008. International*, volume 1, pages 77 –80, October 2008.

[27] Fride Vullum and Dale Teeters. Investigation of lithium battery nanoelectrode arrays and their component nanobatteries. *Journal of Power Sources*, 146(1-2):804 – 808, 2005.

[28] D Pech, M Brunet, H Durou, P Huang, V Mochalin, Y Gogotsi, PL Taberna, and P Simon. Ultrahigh-power micrometre-sized supercapacitors based on onion-like carbon. *Nature nanotechnology*, 5(9):651–655, September 2010.

[29] Zhong Lin Wang. Towards self-powered nanosystems: From nanogenerators to nanopiezotronics. *Advanced Functional Materials*, 18(22):3553–3567, 2008.

[30] Sheng Xu, Benjamin J. Hansen, and Zhong Lin Wang. Piezoelectric-nanowire-enabled power source for driving wireless microelectronics. *Nature Communications*, 1(7):1–5, October 2010.

[31] J. Matthew Dubach, Daniel I. Harjes, and Heather A. Clark. Fluorescent ion-selective nanosensors for intracellular analysis with improved lifetime and size. *Nano Letters*, 7(6):1827–2831, 2007.

[32] Jianping Li, Tuzhi Peng, and Yuqiang Peng. A cholesterol biosensor based on entrapment of cholesterol oxidase in a silicic sol-gel matrix at a prussian blue modified electrode. *Electroanalysis*, 15(12):1031–1037, 2003.

[33] Ibtisam E. Tothill. Biosensors for cancer markers diagnosis. *Seminars in Cell & Developmental Biology*, 20(1):55 – 62, 2009.

[34] Martin Heil and Juan Carlos Silva Bueno. Within-plant signaling by volatiles leads to induction and priming of an indirect plant defense in nature. *Proceedings of the National Academy of Sciences*, 104(13):5467–5472, 2007.

[35] Corn M.J. Pieterse and Marcel Dicke. Plant interactions with microbes and insects: from molecular mechanisms to ecology. *Trends in Plant Science*, 12(12):564 – 569, 2007.

[36] I. F. Akyildiz and J. M. Jornet. The internet of nano-things. *IEEE Wireless Communications Magazine*, 17(6):58–63, December 2010.

[37] I. F. Akyildiz, F. Brunetti, and C. Blazquez. Nanonetworks: A new communication paradigm. *Computer Networks (Elsevier) Journal*, 52(12):2260–2279, August 2008.

[38] Llus Parcerisa and Ian F. Akyildiz. Molecular communication options for long range nanonetworks. *Computer Networks (Elsevier) Journal*, 53(16):2753 – 2766, November 2009.

[39] T. Suda, M. Moore, T. Nakano, R. Egashira, and A. Enomoto. Exploratory research on molecular communication between nanomachines. In *Genetic and Evolutionary Computation Conference (GECCO), Late Breaking Papers*, June 2005.

[40] Massimiliano Pierobon and Ian F. Akyildiz. A physical end-to-end model for molecular communication in nanonetworks. *IEEE Journal of Selected Areas in Communications (JSAC)*, 28(4):602–611, May 2010.

[41] M. Dragoman and D. Dragoman. Graphene-based quantum electronics. *Progress in Quantum Electronics*, 33(6):165 – 214, 2009.

[42] Kyle L. Grosse, Myung-Ho Bae, Feifei Lian, Eric Pop, and William P. King. Nanoscale joule heating, peltier cooling and current crowding at graphenemetal contacts. *Nature Nanotechnology*, 6, 2011.

[43] Liyi Huang, Mitsuhiro Terakawa, Timur Zhiyentayev, Ying-Ying Huang, Yohei Sawayama, Ashlee Jahnke, George P. Tegos, Tim Wharton, and Michael R. Hamblin. Innovative cationic fullerenes as broad-spectrum light-activated antimicrobials. *Nanomedicine: Nanotechnology, Biology and Medicine*, 6(3):442 – 452, 2010.

[44] M. Choudhury, Youngki Yoon, Jing Guo, and K. Mohanram. Technology exploration for graphene nanoribbon fets. In *Proc. of ACM/IEEE Design Automation Conference*, pages 272 –277, June 2008.

[45] Xuebei Yang, Guanxiong Liu, Alexander A. Balandin, and Kartik Mohanram. Triple-mode single-transistor graphene amplifier and its applications. *ACS Nano*, 4(10):5532–5538, 2010.

[46] Han Wang, Daniel Nezich, Jing Kong, and Tomas Palacios. Graphene frequency multipliers. *IEEE Electron Device Letters*, 30:547–549, 2009.

[47] Floriano Traversi Roman Sordan and Valeria Russo. Logic gates with a single graphene transistor. *Applied Physics Letters*, 94:073305, 2009.

[48] S. Tanachutiwat. Reconfigurable multi-function logic based on graphene pn junctions source. In *Proceedings of the 47th Design Automation Conference on - DAC '10*, 2010.

[49] Josep Miquel Jornet and Ian F. Akyildiz. A nano-patch antenna for electromagnetic nanocommunications in the terahertz band. *Broadband Wireless Networking Lab Technica*, 2009.

[50] et al. Yu-Ming Lin. Operation of graphene transistors at gigahertz frequencies. *Nano letters*, 9:422–426, 2009.

[51] E. R. Mueller, Jr. W. E. Robotham, R. P. Meisner, R. A. Hart, J. Kennedy, and L. A. Newman. 2.5 thz laser local oscillator for the eos chem 1 satellite. In *Proceedings 9th Int. Space Terahertz Technology Symposium*, 1998.

[52] M. Dragoman and A.A. Dragoman, D.and Muller. High frequency devices based on graphene. In *International Semiconductor Conference (CAS)*, volume 1, pages 53 –56, 15 2007-Sept. 17 2007.

[53] L. Berger. Emission of spin waves by a magnetic multilayer traversed by a current. *Physical Reviews B*, 54:9353–9358, 1996.

[54] Alma E. Wickenden, Chris Fazi, Ben Huebschman, Roger Kaul, Andrew C. Perrella, William H. Rippard, and Matthew R. Pufall. Spin torque nano oscillators as potential terhertz (thz) communications devices. Technical report, Army Research Laboratory, 2009.

[55] Shehzaad Kaka, Matthew R. Pufall, William H. Rippard, Thomas J. Silva, Stephen E. Russek, and Jordan A. Katine. Mutual phase-locking of microwave spin torque nano-oscillators. *Nature*, 437:389–392, 2005.

[56] M. A. Hoefer, M. J. Ablowitz, B. Ilan, M. R. Pufall, , and T. J. Silva. Theory of magnetodynamics induced by spin torque in perpendicularly magnetized thin films. *Physical Review Letters*, 95:267206, 2005.

[57] Peter H. Siegel. Terahertz technology. *IEEE Transactions on Microwave Theory and Techniques*, 50(3):910–928, March 2002.

[58] S. A. Mikhailov and K. Ziegler. Nonlinear electromagnetic response of graphene: Frequency multiplication and the self-consistent-field effects. *Journal of Physics*, 20:384204 (10pp), 2008.

[59] Farhan Rana. Graphene terahertz plasmon oscillators. *IEEE Transactions on Nanotechnology*, 7:91–99, 2008.

[60] I. F. Akyildiz, J. M. Jornet, and M. Pierobon. Propagation models for nanocommunication networks. In *Proc. of EUCAP 2010, Fourth European Conference on Antennas and Propagation (invited paper), Barcelona, Spain*, April 2010.

[61] Sachiko Nakajima, Hiromichi Hoshina, Masatsugu Yamashita, Chiko Otani, and Norio Miyoshi. Terahertz imaging diagnostics of cancer tissues with a chemometrics technique. *Applied Physics Letters*, 90:041102, January 2007.

[62] R. W. McMillan. *Advances in Sensing with Security Applications*, volume 2 of *New York*, chapter Terahertz Imaging, Millimeter-Wave Radar, pages 243–268. Springer, 2006.

[63] R.M. Goody and Yung Y.L. *Atmospheric Radiation: Theoretical basis*. Oxford University Press, 1989.

[64] J. M. Jornet and Ian F. Akyildiz. Low-weight channel coding for interference mitigation in electromagnetic nanonetworks in the terahertz band. In *to appear in Proc. of IEEE International Conference on Communications, ICC*, pages 1–6, June 2011.

[65] J. M. Jornet and I. F. Akyildiz. Capacity of pulse-based electromagnetic nanonetworks in the terahertz band. *submitted for conference publication*, July 2010.

[66] M. Rosenau da Costa, O. V. Kibis, and M. E. Portnoi. Carbon nanotubes as a basis for terahertz emitters and detectors. *Microelectronics Journal*, 40(4-5):776–778, April 2009.

[67] A. Gerosa, S. Solda, A. Bevilacqua, D. Vogrig, and A. Neviani. An energy-detector for noncoherent impulse-radio uwb receivers. *IEEE Transactions on Circuits and Systems I: Regular Papers*, 56(5):1030 –1040, May 2009.

[68] F.S. Lee and A.P. Chandrakasan. A 2.5 nj/bit 0.65 v pulsed uwb receiver in 90 nm cmos. *IEEE Journal of Solid-State Circuits*, 42(12):2851 –2859, December 2007.

[69] P.P. Mercier, M. Bhardwaj, D.C. Daly, and A.P. Chandrakasan. A low-voltage energy-sampling ir-uwb digital baseband employing quadratic correlation. *IEEE Journal of Solid-State Circuits*, 45(6):1209 –1219, june 2010.

[70] S. Iida, K. Tanaka, H. Suzuki, N. Yoshikawa, N. Shoji, B. Griffiths, D. Mellor, F. Hayden, I. Butler, and J. Chatwin. A 3.1 to 5 ghz cmos dsss uwb transceiver for wpans. In *Proc of IEEE International Solid-State Circuits Conference*, pages 214 –594 Vol. 1, February 2005.

[71] T. Norimatsu, R. Fujiwara, M. Kokubo, M. Miyazaki, A. Maeki, Y. Ogata, S. Kobayashi, N. Koshizuka, and K. Sakamura. A uwb-ir transmitter with digitally controlled pulse generator. *IEEE Journal of Solid-State Circuits*, 42(6):1300 –1309, June 2007.

[72] J. Pujol-Capdevila, J. M. Jornet, and J. Sole-Pareta. Phlame: A physical layer aware mac protocol for electromagnetic nanonetworks. In *Proc. of 1st IEEE International Workshop on Molecular and Nano Scale Communication (MoNaCom), INFOCOM, Shanghai, China*, April 2011.

[73] D.D. Wentzloff, F.S. Lee, D.C. Daly, M. Bhardwaj, P.P. Mercier, and A.P. Chandrakasan. Energy efficient pulsed-uwb cmos circuits and systems. In *Proc. of IEEE International Conference on Ultra-Wideband*, pages 282 –287, September 2007.

[74] P.A. Humblet and M. Azizoglu. On the bit error rate of lightwave systems with optical amplifiers. *Journal of Lightwave Technology*, 9(11):1576 –1582, November 1991.

[75] R.F. Mills and G.E. Prescott. A comparison of various radiometer detection models. *IEEE Transactions on Aerospace and Electronic Systems*, 32(1):467 –473, jan. 1996.

[76] H. F. Engler and D. H. Howard. A compendium of analytic models for coherent and noncoherent receivers. Technical report, AFWAL-TR-85-1118, Air Force Wright Aeronautical Laboratory,, September 1985.

[77] S. Marinkovic and E. Popovici. Nano-power wake-up radio circuit for wireless body area networks. In *Proc. of IEEE Radio and Wireless Symposium (RWS)*, pages 398 –401, January 2011.

[78] Wei Ye, J. Heidemann, and D. Estrin. An energy-efficient mac protocol for wireless sensor networks. In *Proc. of 21st Annual Joint Conference of the IEEE Computer and Communications Societies. INFOCOM*, volume 3, pages 1567 – 1576 vol.3, 2002.

[79] Joseph Polastre, Jason Hill, and David Culler. Versatile low power media access for wireless sensor networks. In *Proceedings of the 2nd international conference on Embedded networked sensor systems. SenSys '04*, 2004.

[80] N.P. Khan and C. Boncelet. Pmac: Energy efficient medium access control protocol for wireless sensor networks. In *Military Communications Conference, 2006. MILCOM 2006. IEEE*, pages 1 –5, oct. 2006.

[81] N.M. Pletcher, S. Gambini, and J. Rabaey. A 52 μw wake-up receiver with -72 dbm sensitivity using an uncertain-if architecture. *Solid-State Circuits, IEEE Journal of*, 44(1):269 –280, jan. 2009.